C.P. No. 971

C.P. No. 971

MINISTRY OF TECHNOLOGY

AERONAUTICAL RESEARCH COUNCIL

CURRENT PAPERS

Potential Flow Theory for Tandem Cascade by Howell's Method

by

Y. M. Yip and J. W. Railly

LONDON: HER MAJESTY'S STATIONERY OFFICE

1967

PRICE 9*s* 6*d* NET

Aeronautical Research Council

ERRATA — C.P. No. 971

Potential Flow Theory for Tandem Cascade by Howell's Method

By Y. M. Yip* and J. W. Railly

Page 4, equation (2 6) should read

$$\zeta_2 = \left(\frac{z_2}{2}\right) \pm \sqrt{\left(\frac{z_2}{2}\right)^2 - c_2^2}$$

Page 6, lines 21 and 22 should read

$$V = fC_a + gWu_1 + hWu_2 + jk_1 + lW_{21}\left|a^2 e^{-i\alpha 21} - a_1 e^{i\alpha 21}\right| \cdot \left|\frac{d\zeta}{dz}\right|_s$$

$$\text{or } \frac{V}{C_a} = f + gt_1 + ht_2 + jk_1 + lct_{21} \qquad (3\ 1)$$

Page 7, line 5 should read

$$l = \text{Im part of } \frac{1}{2\pi r}\left[\frac{-e^{i\lambda}}{(1 - m_3\, e^{i\beta 3})} + \frac{e^{i\lambda}}{m_3^2\left(1 - \frac{1}{m_3}\, e^{i\beta 3}\right)^2}\right] \left|\frac{d\zeta}{dz}\right|_s$$

Page 8, equation (3.3) should read

$$\left|\frac{d\zeta}{dz}\right| = \left|\frac{d\zeta_1}{dz_1}\right| \cdot \left|\frac{d\zeta_2}{dz_2}\right| \cdot \left|\frac{d\zeta_4}{dz_4}\right|$$

Page 8, equation (3 4) should read

$$\frac{V}{V_1} = \frac{V}{C_a}\frac{C_a}{V_1}\frac{1}{r} = \frac{V}{C_a}\frac{\cos\alpha_1}{r}$$

Page 8, equation (3 6) should read

$$\frac{V}{C_a} = f + gt_1 + ht_2 + j'k_1 + l'ct_{21}$$

Page 8, equation (3 7) should read

$$L_2 = \rho\, V_s\, K_2$$

Page 9, line 5 should read

is divided into two parts Program 1 covers the initial transformations up to

Page 9, line 6 should read

the last of Joukowski transformation Part 2 completes the final or Theodorsen

Page 9, line 23 should read

4 1 2 "tanh" transformation (Chapter 0 of program)

Page 10, line 10 should read

The first part of Chapter 2 of the program locates the major axis of

Page 10, equation (2.7) should read

$$\zeta_3 = \left(\frac{z_3}{2}\right) \pm \sqrt{\left(\frac{z_3}{2}\right)^2 - c_3^2}$$

Page 14, line 13 should read

Chapters 0 and 1 of Program 2 contain the above calculations

Page 15, equation (5 16) should read

$$\lambda - \psi = \sum_{k=1}^{n}\left[A_n' \frac{e^{n\psi 0}}{e^{n\psi}} \cos n\theta + B_n' \frac{e^{n\psi 0}}{e^{n\psi}} \sin\theta\right]$$

Page 18, line 19 should read

c modulus of $(a^2 e^{-i\alpha 21} - a_1 e^{i\alpha 21})$

---

* Now at the English Electric Co Ltd , Mechanical Engineering Laboratories, Whetstone, Leicester

Ministry of Technology
Aeronautical Research Council
National Physical Laboratory
December 1967

LONDON: HER MAJESTY'S STATIONERY OFFICE

(96923) Dd 129528 K 4 1/68 Hw

C.P. No. 971*

December, 1965

Potential Flow Theory for Tandem Cascade by Howell's Method

- By -
Y. M. Yip and J. W. Railly,
University of Birmingham

Department of Mechanical Engineering
Research Report No. 56

List of Contents

6./

*Replaces A.R.C. 27 510.

---

1. Introduction

As in the case of single cascade, the potential theory of tandem cascade can be divided into two main categories, one using the method of singularities and the other using the method of conformal transformation. Various workers[9,11] have used the method of singularities, but these are approximate only. The method of conformal transformation offers the only exact method. Spraglin[12] has stated rigorously the method of conformal transformation applied to a tandem cascade. In this method the two rows of blades are transformed, through two intermediate stages (namely two rows to two irregular shapes, then to two circles) to two concentric circles, with two singularities within the annulus formed between the circles. The method of mirror images is then employed to solve the flow in the annulus. The main difficulty arises when the two singular shapes are transformed into two circles.

The method employed here by the authors is not an exact method but intermediate between the two mentioned above. On the assumptions that the main blade carries the bulk of the loading and the second blade acts as a flow deflector, the emphasis is on the investigation of the loading on the first blade and the effect on it of circulation of the second blade. Accordingly, the tandem cascade is "separated" into two parts, the first row of blades is transformed into a circle while the second is represented by a singularity. The whole transformation is based exclusively on Howell's method which is explained in Section 2. Regarding the representation of the singularity, two studies are included. The first study only takes account of the circulation effect which is represented by a vortex. The second study includes the effect of blade thickness which is represented by a doublet. A numerical example for the first study is included in this report (Sections 4 and 5).

In applying the transformations by Howell's method, it has been the authors' aim to achieve a completely automatic process by digital computer for numerical solution from which the pressure distribution can be obtained when the basic profile is fed in. The main difficulty in using Howell's method arises in the transformation from a near circle to an exact circle, which is carried out by means of the Kármán-Theodorsen transformation[3,13]. In this report, the numerical method to overcome such difficulties and the programming technique is described in full detail.

The digital computer program is divided into two parts, written in "Mercury Autocode"[1]. The first part deals with the initial transformations and

requires/

requires 3 minutes on Ferranti "Mercury" Computer (can also be run on "Atlas" or English Electric "KDF 9"). The second part which deals with the final transformation and pressure distribution requires approximately 40 seconds of computing time. (The actual time required in computing time plus time taken for input blocks.) This part can only be accepted by Ferranti "Atlas" computers in the form in which it has been programmed.

Sections 2 and 3 deal with the theory of transformation. Details of programming techniques and numerical applications are described in Sections 4 and 5. Two numerical examples are given in Section 6.

2. The Conformal Transformation

2.1 Potential flow

The problem of the tandem cascade is assumed to be of two-dimensional, incompressible and inviscid flow. The flow in z-plane satisfies the following:

Cauchy-Riemann equation:

$$\left.\begin{aligned} u &= \frac{\partial \phi}{\partial x} = \frac{\partial \psi}{\partial y} \\ v &= \frac{\partial \phi}{\partial y} = -\frac{\partial \psi}{\partial x} \end{aligned}\right\} \qquad \ldots(2.1)$$

Potential function: $W = \phi + i\psi$ $\qquad \ldots(2.2)$

Velocity function: $w = u - iv.$ $\qquad \ldots(2.3)$

2.2 Outline of the method

The conformal transformation method employed here is based on the Howell's method, assuming the chord of the second blade is not greater than a quarter of the combined chord, i.e., $C_2 \leq 0{\cdot}25C$. The second blade is then replaced by a singularity at the position of maximum thickness on its camber line. Its effect is represented by a vortex either with or without a doublet[6]. After the substitution, the tandem cascade is reduced to a single cascade with a row of singularities and can be dealt with as an ordinary cascade (Figs. 1 and 2).

The first transformation function used is $\zeta_1 = \tanh z_1$ which, having a period of π, transforms the cascade into an "S" shape (Fig. 4). This transformation introduces two singularities at ± 1 points in ζ_1 plane corresponding to the points at $\pm\infty$ in the z_1-plane. Two successive applications of Joukowski's transformations turn the "S" shape into a near oval and then to a near circle. In most cases, this near circle can readily be transformed into a true circle by means of the Theodorsen transformation. The method of images is used to solve the flow about the circle. The strength of the singularities do not alter throughout the processes of transformation except for the doublet which depends on the resultant coefficient of transformation.

2.3 The "tanh" transformation: $\zeta_1 = \tanh z_1$

This transformation which maps the first blade having a pitch π into an "S" shaped figure is written as

ζ_1/

$$\zeta_1 = \frac{e^{2z_1} - 1}{e^{2z_1} + 1} \qquad \ldots(2.4)$$

and its transformation coefficient is

$$\frac{d\zeta_1}{dz_1} = 1 - \zeta_1^2. \qquad \ldots(2.5)$$

As pointed out in the last paragraph, the $(\pm\infty, 0)$ points in the z_1-plane are mapped to the $(\pm 1, 0)$ points in the ζ_1-plane. It can be shown that singularities here of a definite type correspond to the uniform flow conditions upstream and downstream of the cascade as follows: at the $(-1,0)$ point in the ζ_1-plane, the potential function is represented by a source of πCa and a vortex (in anti-clockwise direction) of strength πWu_1. Similarly, at the $(1,0)$ point in the ζ_1-plane, the potential function is represented by a source of strength πCa and a vortex (in clockwise direction) of strength πWu_2. In addition, the circulation $\pi(Wu_1 - Wu_2)$ remains unchanged around the configuration.

Regarding the representation of the second blade, its location must be determined before the transformation. The vortex is of strength πk_1 where k_1 is an arbitrary value. The strength of the doublet is determined graphically and represented by $V(a^2 e^{-i\alpha} - a_1 e^{i\alpha})$. The meanings of the symbols of this expression can be found in Fig. 3.

For different relative positions of the second blade, different positions for the singularity must be predetermined.

2.4 The Joukowski transformation

$$z_2 = \zeta_2 + \frac{c_2^2}{\zeta_2}$$

or

$$\zeta_2 = \left(\frac{z_2}{2}\right) \pm \sqrt{\left(\frac{z_2}{2}\right)^2 + c_2^2} \qquad \ldots(2.6)$$

where c_2 is defined as a quarter of the distance joining the centres of curvature at leading and trailing edges. This will produce a near oval shape. The third transformation is similar to the above one.

$$\zeta_3 = \left(\frac{z_3}{2}\right) \pm \sqrt{\left(\frac{z_3}{2}\right)^2 - c_3^2} \qquad \ldots(2.7)$$

where ζ_3 is now the quarter distance between the centres of curvature of the configuration by the major axis.

Before performing these transformations, suitable axes of the configuration have to be obtained (see Figs. 4 and 5).

The/

The transformation coefficients are:-

$$\frac{d\zeta_2}{dz_2} = \frac{\zeta_2^2}{\zeta_2^2 - c_2^2} \qquad \ldots(2.8)$$

and

$$\frac{d\zeta_3}{dz_3} = \frac{\zeta_3^2}{\zeta_3^2 - c_3^2}. \qquad \ldots(2.9)$$

2.5 The Kármán-Theodorsen transformation

The approximate circle is transformed to a true circle by means of this well-known transformation of

$$\log \frac{z_4}{\zeta_4} = \frac{A_n + iB_n}{\zeta_4^n} \qquad \ldots(2.10)$$

where z_4 (near circle) $= ae^{\lambda+i\phi}$ $\qquad \ldots(2.11)$

and ζ_4 (exact circle) $= ae^{\psi+i\theta}$ $\qquad \ldots(2.12)$

The areas in both planes are assumed to be the same. From equations (2.11) and (2.12)

$$(\lambda - \psi) + i(\phi - \theta) = \sum_1^n (A_n + iB_n) \frac{\cos n\theta - i\sin n\theta}{(ae^{\psi})^n}.$$

Separating real and imaginary parts

$$\Delta \equiv \lambda - \psi = \sum_1^n \left(\frac{1}{ae^{\psi}}\right)^n (A_n \cos n\theta + B_n \sin n\theta) \qquad \ldots(2.13)$$

and

$$\epsilon \equiv \phi - \theta = \sum_1^n \left(\frac{1}{ae^{\psi}}\right)^n (B_n \cos n\theta - A_n \sin n\theta). \qquad \ldots(2.14)$$

From (2.13) the following Fourier series equations can be deduced:-

$$\psi_o = \frac{1}{2\pi}\int_o^{2\pi} \lambda_o d\theta \qquad \ldots(2.15)$$

$$A_n' = \frac{A_n}{(ae^{\psi_o})^n} = \frac{1}{\pi}\int_o^{2\pi} \lambda_o \cos n\theta d\theta \qquad \ldots(2.16)$$

$$B_n' = \frac{B_n}{(ae^{\psi_o})^n} = \frac{1}{\pi}\int_o^{2\pi} \lambda_o \sin n\theta d\theta. \qquad \ldots(2.17)$$

Suffix o denotes the values in the original z_4 plane. Assuming θ is very near to ϕ, ψ_o A_n' and B_n' can easily be found. The disadvantages

of/

of this assumption will be discussed more fully in Section 5. It may be noted that the ψ_o will be zero if the area of the near and exact circles are equal.

For singularities ψ can be found from

$$\lambda - \psi = \sum_{1}^{n} \left(A'_n \frac{e^{n\psi_o}}{e^{n\psi}} \cos n\theta + B'_n \frac{e^{n\psi_o}}{e^{n\psi}} \sin n\theta \right) \qquad \ldots(2.13a)$$

by iterating ψ until both sides of the equation become equal. Then the angular difference can be obtained from

$$\phi - \theta = \sum_{1}^{n} \left(B'_n \frac{e^{n\psi_o}}{e^{n\psi}} \cos n\theta - A'_n \frac{e^{n\psi_o}}{e^{n\psi}} \sin n\theta \right). \qquad \ldots(2.14a)$$

From equations (2.11) and (2.12) the expression for the velocity coefficient can be developed. Rewriting the equations:

$$z_4 = ae^{\lambda+i\phi} \qquad \ldots(2.11)$$

$$\zeta_4 = ae^{\psi+i\theta}. \qquad \ldots(2.12)$$

Hence

$$\left| \frac{d\zeta_4}{dz_4} \right| = \left| \frac{\zeta_4}{z_4} \right| \cdot \frac{1 - (d\epsilon/d\phi)}{\sqrt{1 + (d\lambda/d\phi)^2}}. \qquad \ldots(2.18)$$

Assuming ϵ is small so that the squares and higher powers of $d\epsilon/d\phi$ and $d\lambda/d\phi$ can be neglected, Howell argues that

$$\frac{d\zeta_4}{dz_4} = 1 + \sum_{1}^{n} [(n-1)A'_n \cos n\theta_o + (n-1)B'_n \sin n\theta_o]. \qquad \ldots(2.19)$$

3. Pressure Distribution

3.1 Velocity on circle

The velocity on the aerofoil points can easily be calculated on the circle using the method of images (Fig. 7). Referring to Howell's paper, it can be summarised as follows:

$$u = fC_a + gWu_1 + hWu_2 + jk_1 + \ell W_{21} \left| a^2 e^{-i\alpha_{21}} - a_4 e^{i\alpha_{21}} \right| \cdot \left| \frac{d\zeta}{dz} \right|_s$$

or

$$\frac{v}{C_a} = f + gt_1 + ht_2 + j\bar{k}_1 + \ell c t_{21} \qquad \ldots(3.1)$$

where/

where f = Im part of $\frac{1}{2r}\left[\frac{1}{1 - m_1 e^{i\beta_1}} + \frac{1}{1 - \frac{1}{m_1} e^{i\beta_1}} - \frac{1}{1 - m_2 e^{i\beta_2}} - \frac{1}{1 - \frac{1}{m_2} e^{i\beta_2}}\right]$

g = Im part of $\frac{-i}{2r}\left[\frac{1}{1 - m_1 e^{i\beta_1}} - \frac{1}{1 - \frac{1}{m_1} e^{i\beta_1}}\right]$

h = Im part of $\frac{i}{2r}\left[\frac{1}{1 - m_2 e^{i\beta_2}} - \frac{1}{1 - \frac{1}{m_2} e^{i\beta_2}}\right]$

j = Im part of $\frac{i}{2\pi r}\left[1 + \frac{1}{1 - m_3 e^{i\beta_3}} - \frac{1}{1 - \frac{1}{m} e^{i\beta_3}}\right]$

ℓ = Im part of $\frac{1}{2\pi r}\left[\frac{-e^{i\lambda}}{(1 - m_3 e^{i\beta_3})} + \frac{e^{-i\lambda}}{m_3^2\left(1 - \frac{1}{m_3} e^{i\beta_3}\right)^2}\right] \cdot \left|\frac{d\zeta}{dz}\right|_s$

c = modulus of $(a^2 e^{-i\alpha_{21}} - a_1 e^{i\alpha_{21}})$.

It can be seen that there are three unknowns in equation (3.1) which is solved in two steps. Firstly, by neglecting the effect of the second blade, the outlet angle and velocity α_{21} and W_{u21} can be found by satisfying the Joukowski hypothesis that the velocity at the first trailing edge is zero.

Rewriting equation (3.1) we have

$$f + gt_1 + ht_{21} = 0. \qquad \ldots(3.2)$$

Thus the coefficient which introduced the doublet effect of the second blade can be then calculated.

The second step is to assume an arbitrary α_2 for the corresponding α_1; this will impose a certain $\bar{k}_1$, the strength of the vortex. Consequently, the ratio of circulation can be evaluated in relation to the lift coefficient of the first blade.

In the case where the thickness effect is neglected, the last term in equation (3.1) becomes zero. Then $\bar{k}_1$ can be calculated by assuming α_2.

3.2 Pressure distribution

The velocity on this profile is found from the relation

$$V_{profile} = V_{circle} \times \left|\frac{d\zeta}{dz}\right|$$

where/

where $$\left|\frac{d\zeta}{dz}\right| = \left|\frac{d\zeta_1}{dz}\right| \cdot \left|\frac{d\zeta_2}{dz_2}\right| \cdot \ldots\ldots \cdot \left|\frac{d\zeta_4}{dz_4}\right|. \qquad \ldots(3.3)$$

Hence $$\frac{V}{V_1} = \frac{V}{C_a}\frac{C_a}{V_1}\frac{1}{r} = \frac{V_r}{C_a}\frac{\cos\alpha_1}{r}. \qquad \ldots(3.4)$$

Therefore, the pressure distribution around the aerofoil will be

$$\frac{p - p_1}{\frac{1}{2}\rho V_1} = 1 - \left(\frac{V}{V_1}\right)^2. \qquad \ldots(3.5)$$

3.3 Lift coefficient of the second blade

The velocity of the substantial singularity is calculated from an expression similar to equation (3.1) with modified j and ℓ terms to exclude the singularity effect generated by itself. The modified terms are

$$j' = \text{Im part of } \frac{i}{2\pi r}\left[1 - \frac{1}{\frac{1}{m^2}e^{i\beta_2}}\right]$$

$$\ell' = \text{Im part of } \frac{1}{2\pi r} \times \frac{e^{-i\lambda}}{m_2^2\left(1 - \frac{1}{m_2}e^{i\beta_2}\right)^2}.$$

Therefore the complete velocity expression for this singularity point is

$$\frac{V}{C_a} = f + gt_1 + ht_2 + j'\bar{K}_1 + \ell' ct_{21}. \qquad \ldots(3.6)$$

Hence the lift can be found from

$$L_2 = \rho V K_2. \qquad \ldots(3.7)$$

4. Numerical Applications, Part 1

Various research workers have attempted to solve this series of transformation by different techniques. Carter and Hughes[2] carried out their investigations by hand calculations, choosing 12 aerofoil points. Recently Pollard and Wordsworth[10] used the "Deuce" digital computer to compute the transformations. In the latter method, each transformation had to be computed separately.

The/

The aim herein is to provide firstly a satisfactory way to handle the transformations automatically, secondly a method which will give better approximations. All refinements are described under separate headings. Due to the limitation of the use of computer facilities, the complete Howell's method is divided into two parts. Program I covers the initial transformations up to the last of Joukowski transformation. Part II completes the final or Theodorsen transformation and pressure distribution. The two programs were written primarily for development and therefore some instructions in the present form are redundant for production. These instructions are, however, very useful for checking at intermediate stages should it be required. The input index "R" governs such a process.

4.1 Program 1

4.1.1 Input data

Data required for the program are the number of aerofoil points, total number of points for computation, stagger, relative position of the origin in z_1 plane (about 40% chord), chord length, pitch to chord ratio and finally x and y co-ordinates of the aerofoil points.

The locations of the $(\pm\infty, 0)$ points are not required but since we know that after the first transformation they will fall on $(\pm 1, 0)$ therefore only the latter are fed in. In regard to the number and locations of substitutional singularities for each stagger, these must be decided graphically and the co-ordinates should be included in the data.

4.1.2 "tanh" transformation (Chapter 0 of programme)

Before the transformation, the aerofoil points are translated to the new axes and rotated to the corresponding stagger. At the same time, all co-ordinates are referred to the correct pitch to chord ratio with a pitch π. The computation of transformation and velocity coefficients follows, taking the form of:-

$$\zeta_1 = \frac{e^{2z_1} - 1}{e^{2z_1} + 1}$$

and

$$\left| \frac{d\zeta_1}{dz_1} \right| = |1 - \zeta_1^2|.$$

The calculation of the points $(\pm\infty, 0)$ is excluded in order to avoid overflowing the capacity of the computer.

Then the centre of curvature of the leading edge is calculated while that for the trailing edge is of course the trailing edge itself. The co-ordinates in the ζ_1-plane are transferred to the z_2-plane. The value of c_2 is also calculated.

4.1.3/

4.1.3 Joukowski transformation (Chapter 1)

This transformation takes the form of

$$\zeta_2 = \left(\frac{z_2}{2}\right) \pm \sqrt{\left(\frac{z_2}{2}\right)^2 - c_2^2} \qquad \ldots(2.6)$$

and

$$\left|\frac{d\zeta_2}{dz_2}\right| = \left|\frac{\zeta_2^2}{\zeta_2^2 - c_2^2}\right|. \qquad \ldots(2.8)$$

It is essential that the signs in equation (2.6) be taken correctly. In order to obtain a continuous loop, the positive and negative signs are used for the suction and pressure surfaces respectively. The choice of sign for the singularities follow the sign of y_2 of the point considered. The result of the second transformation is a near oval shape.

The first part of Chapter 2 of the programme locates the major axis of the ellipse by comparing the lines joining all the co-ordinates. The first step is to find the points which give the longest distance between them. The centre of curvature are located by assuming a circular arc passing through two points adjacent to each of these two points. The line joining the centres of curvature gives the x_3-axis in the z_3-plane and the centre between them the origin. The value c_3 is a quarter of the distance between these two centres.

About this origin, the near oval is translated and rotated. The calculation is directed to jump back to Chapter 1 of the program to perform the second Joukowski's transformation, namely:-

$$\zeta_3 = \left(\frac{z_3}{2}\right) \pm \sqrt{\left(\frac{z_3}{2}\right)^2 + c_3^2} \qquad \ldots(2.7)$$

and

$$\left|\frac{d\zeta_3}{dz_3}\right| = \frac{|\zeta_3^2|}{|\zeta_3^2 - c_3^2|}. \qquad \ldots(2.9)$$

The choice of sign presents no difficulty this time. The plus or minus sign follows that of the y-co-ordinates of the point concerned.

The program ends at this stage, and it requires three minutes on the "Mercury" computer if the output is limited to the third transformation. Fig. 8 shows the block diagram of this program.

4.1.4 Results

The print-out of the results is given in the following form:-

Co-ordinates after the first transformation and its coefficients

Value of c_2

Co-ordinates/

Co-ordinates after the second transformation and product of coefficients

Value of c_s

Number of points around aerofoil

Total number of points involved

Co-ordinate after third transformation and product of coefficients.

It is designed so that the results (of the third transformation) may be fed straight into Program 2. Results of any individual transformation may be plotted, using the output tape, by the Friden, a suitable automatic plotter.

5. Numerical Application, Part 2

5.1 Program 2

This program deals with the final transformation and pressure distribution on the blade surface.

The importance of the numerical application of the Theodorsen transformation need not be overemphasised. In fact, the Howell's method hinges on the successful evaluations of this transformation and its coefficients.

The method used in this report differs distinctly from those adapted by Carter and Hughes[2], Pollard and Wordsworth[10], Thwaites[14] and Naiman[7,8]. Fourier coefficients are calculated, using input aerofoil points, by analytical integration. The usual assumption of $\phi \simeq \theta$ is eliminated by a process of iteration. Finally, the numerical differentiation is carried out by a specially developed curve fitting programme for five points, two on each side of the point concerned.

5.2 Theodorsen transformation

The equations for the Theodorsen transformation may be summarised as follows:-

$$z_4 \text{ (near circle)} = ae^{\lambda+i\phi} \qquad \ldots(5.1)$$

$$\zeta_4 \text{ (true circle)} = ae^{\psi+i\theta} \qquad \ldots(5.2)$$

$$\Delta \equiv \lambda - \psi = \sum_{1}^{n} \left(\frac{1}{ae^{\psi}}\right)^{n} (A_n \cos n\theta + B_n \sin n\theta) \qquad \ldots(5.3)$$

$$\varepsilon \equiv \phi - \theta = \sum_{1}^{n} \left(\frac{1}{ae^{\psi}}\right)^{n} (B_n \cos n\theta - A_n \sin n\theta) \qquad \ldots(5.4)$$

$$\psi_o = \frac{1}{2\pi}\int_{o}^{2\pi} \lambda_o d\theta \qquad \ldots(5.5)$$

A_n'/

$$A'_n = \frac{A_n}{(ae^{\psi_o})^n} = \frac{1}{\pi}\int_o^{2\pi} \lambda_o \cos n\theta \, d\theta \qquad \ldots(5.6)$$

$$B'_n = \frac{B_n}{(ae^{\psi_o})^n} = \frac{1}{\pi}\int_o^{2\pi} \lambda_o \sin n\theta \, d\theta. \qquad \ldots(5.7)$$

Various attempts have been made by others to determine the Fourier coefficients in these equations. The main assumption made is that ϕ can be used for θ in evaluating A'_n and B'_n. Carter and Hughes[2] suggest using three terms with eight values of λ at equal intervals of the argument. Naiman[7,8] introduces the use of harmonic analysis to solve equation (5.4). Thwaites[14], making use of Watson's formulae[15] uses a matrix method to solve the equations. All these methods state that absolute convergence of the Fourier series can be obtained. But the drawbacks are firstly that difficulties arise in copying with the irregularities in shape on the near circle. Secondly, equal intervals of ϕ (instead of θ) must be used, whilst the validity of the assumption $\phi \simeq \theta$ is questionable. The convergence of the Fourier series depends on whether the curve possesses any shape irregularity. In an ordinary cascade, a "bump" at the leading-edge point has a predominant effect on the convergence of the series. To by-pass this effect, Pollard and Wordsworth[10] leave this point out throughout the entire calculation of the series. The questions left to be answered are: what happens if there is more than one dominating irregularity and what effect has the "left-out" calculation on the other profile points. With an unusual profile which is most likely for a tandem cascade such as the one used in this report, it is possible that errors may result.

To counter the above-mentioned difficulties, the following method is used:-

(a) Calculation of the Fourier series coefficients by analytical integration instead of summation.

(b) Use of the original aerofoil points throughout (this is to avoid using an interpolation method).

(c) Elimination of the assumption of $\phi \simeq \theta$ by a process of iteration.

5.2.1 Evaluation of ψ_o

The sequence of input data is:-

The number of aerofoil points.

Total number of points including singularities.

Co-ordinates in the sequence of number, x-co-ordinate, y-co-ordinates and product of transformation coefficients.

With the help of the plot-out of the last Joukowski transformation, a new origin nearest to the "centre" of the near circle may be easily selected.

Assuming that the areas of the near and true circles are equal, the radius of the base circle can best be found by taking the average value of the radii: thus

a/

$$a = \frac{1}{p} \sum_{1}^{p} \lambda_o . \qquad \ldots(5.8)$$

The value of ψ_o may be found from:-

$$\psi_o = \frac{1}{2\pi} \int_o^{2\pi} \lambda_o \, d\theta = \frac{1}{2\pi} \sum_{1}^{p} \lambda_o \left[\theta(p+\tfrac{1}{2}) - \theta(p-\tfrac{1}{2})\right] \qquad \ldots(5.9)$$

where p = number of aerofoil points.

5.2.2 Fourier coefficients

The integrals in the equations for A_n' and B_n' represent the areas under the $\lambda_o \cos n\theta$ and $\lambda_o \sin n\theta$ curves respectively. It is possible to write approximately,

$$A_n' = \frac{1}{\pi} \int_o^{2\pi} \lambda_o \cos n\theta \, d\theta = \frac{1}{\pi} \sum_{k=1}^{p} \lambda_k \cos n\theta_k \, \delta\theta_k \qquad \ldots(5.10)$$

$$B_n' = \frac{1}{\pi} \int_o^{2\pi} \lambda_o \sin n\theta \, d\theta = \frac{1}{\pi} \sum_{k=1}^{p} \lambda_k \sin n\theta_k \, \delta\theta_k . \qquad \ldots(5.11)$$

However, these expressions and hence the coefficients, become increasingly unreliable as n increases beyond one eighth of the number, p, describing the near circle.

The method described in this report proceeds as follows. With a sufficient number of aerofoil points (48 proved to be satisfactory) describing the near circle, it may be assumed that λ is a linear function of θ between adjacent points. Hence

$$A_n' = \frac{1}{\pi} \int_o^{2\pi} (m\theta+c) \cos n\theta \, d\theta \qquad \ldots(5.12)$$

$$B_n' = \frac{1}{\pi} \int_o^{2\pi} (m\theta+c) \sin n\theta \, d\theta \qquad \ldots(5.13)$$

where m and c are constants pertaining to a short straight line joining adjacent points. Dividing the $\lambda - \theta$ diagram into small strips, it may be shown that after carrying out the above integration analytically, the coefficients are given by:-

A_n'/

$$A'_n = \frac{1}{\pi n^2} \sum_{k=1}^{p} (m_k - m_{k+1}) \cos n\theta_k \qquad \ldots(5.12a)$$

$$B'_n = \frac{1}{\pi n^2} \sum_{k=1}^{p} (m_k - m_{k+1}) \sin n\theta_k \qquad \ldots(5.13a)$$

where m_{k+1} = slope between points k and k+1; if m is less than or equal to unity, the series converges rapidly.

The value of θ is first assumed to be equal to ϕ (near circle); after calculating A'_n and B'_n, ϵ may be evaluated from equation (5.4). If ϵ_1^* denotes this first set of values then the new set of values of θ will be

$$\theta_{s1}^* = \phi - \epsilon_1^*.$$

The value of θ_{s1}^* is then used to recalculate the Fourier coefficients and hence ϵ_2^*. With three iterations, and using 100 terms for each of the coefficients, a final set of values of ϵ^* is produced. Further iteration may cause a change of 0·0002 degrees at some points (see examples 1 and 2).

Chapters 0 and 1 of Program II contain the above calculations.

5.2.3 Coefficients of the last transformation

The second difficulty is the calculation of the velocity coefficients of the final transformation which, in exact form is:-

$$\left| \frac{d\zeta}{dz} \right|_4 = \left| \frac{\zeta_4}{z_4} \right| \cdot \frac{1 - \frac{d\epsilon}{d\phi}}{\sqrt{\left\{ 1 + \left(\frac{d\lambda}{d\phi} \right)^2 \right\}}}. \qquad \ldots(5.14)$$

Howell demonstrates that if the second and higher powers of the differentials of ϵ and λ with respect to ϕ may be neglected, the modulus will be given by:-

$$\left| \frac{d\zeta}{dz} \right|_4 = 1 + \sum_{1}^{n} [(n-1) A'_n \cos n\theta - (n-1) B'_n \sin n\theta]. \qquad \ldots(5.15)$$

The reliability of this equation depends on two factors. The governing one is the rapidity of convergence of the Fourier coefficients. Although equations (5.12a) and (5.13a) always converge, a rapid rate of convergence is obtained only at the beginning of the series. Differentiation

of/

of the series therefore is highly unreliable[5]. Secondly, the large number of Fourier coefficients used to accommodate irregularities become increasingly unstable for numerical differentiation, perversely, over the smooth part of the ε-ϕ and λ-ϕ curve.

The best course appears to be to carry out the differentiation after fitting a polynomial function to the set of values of ε and λ, then values of $d\varepsilon/d\phi$ and $d\lambda/d\phi$ are obtained by ordinary differentiations. In the method described, curve fitting is applied to groups of five points.

5.2.4 Five point curve fitting

The three ways that would be chosen to fit a curve to five points are by the use of fourth order, third order least square and second order least square polynomials. Fig. 10 shows half of the fifty-four possible ways a curve may be drawn through the five points. These exclude the cases with continuous gradients. For any point that may be considered, two adjacent points on each side are used in the process of curve fitting.

From these sketches, it may be seen that none of the above methods can be applied to all points. Therefore, tests must be carried out first to decide which method has to be used for each individual point. Straight lines are drawn between successive points and their gradients determined. The gradients are then compared with each other to find out to which group the five points might belong (e.g., group 1, Fig. 10). For some groups (e.g., group 1) these points have to be rotated and the same tests re-applied. When the order of the curve has been decided, the gradient may easily be found.

An example of the λ-curve for example 1 (Section 6.1) is shown in Fig. 11. The curves fitted to each particular point are shown in Figs. 12A, B, C, D, and E. Chapter 2 of the program deals with curve fitting and the derivative of the curve. Chapter 3 completes the calculation of the coefficients of the Theodorsen transformation. With slight modification Chapter 2 may be used quite separately for five point curve fitting purposes.

5.2.5 Singularities

Chapter 4 of the program obtains the values of ε and ψ for each of the singularity points. Rewriting equations (2.13a) and (2.14a)

$$\lambda - \psi = \sum_{k-1}^{n} \left[A'_n \frac{e^{n\psi_o}}{e^{n\psi}} \cos n\theta + B'_n \frac{e^{n\psi_o}}{e^{n\psi}} \sin \theta \right] \qquad \ldots(5.16)$$

$$\phi - \theta = \sum_{k=1}^{n} \left[B'_n \frac{e^{n\psi_o}}{e^{n\psi}} \cos n\theta - A'_n \frac{e^{n\psi_o}}{e^{n\psi}} \sin n\theta \right] \qquad \ldots(5.17)$$

Thirty terms of A'_n and B'_n are used. The process consists of a double iteration. Commencing with the assumption $\phi = \theta$, equation (5.16) is used to evaluate ψ by successive approximation. When the values of ψ for each singularity have converged, they are substituted into equation (5.17) to

obtain/

obtain θ, whereupon ψ is recalculated. The process is repeated until $\phi - \theta$ is less than 0·001.

For the transformation coefficients the original method has to be employed since neither $d\lambda/d\phi$ nor $d\theta/d\phi$ may be obtained by curve fitting in this case. The relevant equation is:

$$\frac{dz_4}{dz_4} = 1 + \sum_{1}^{n} [(n-1)\, A_n' \cos n\theta - (n-1)\, B_n' \sin n\theta]. \qquad \ldots(5.18)$$

5.3 Velocity and pressure distribution

The final chapter of the program calculates the pressure distribution around the aerofoil using formulae listed in Section 3. In this program, seven values of inlet angles (α_1) are used, from 40 to 70 with 5 degrees interval. These values can of course be changed. It is also necessary to submit a series of values of the outlet angle α_2. This enables the computer to calculate the values of the strength of the substitutional vortex and its proportional circulation.

5.3.1 Results

The results are printed out in block form, giving first the value of α_1, α_2, $\alpha_1 - \alpha_2$ and $\tan\alpha_1 - \tan\alpha_2$. The dimensionless pressure around the profile is then given and is followed by the ratio of circulation.

Should results of the curve fitting part be required correct use of the governing values "B" and "M" in Chapter 2 would direct the print-out.

A Block diagram for this program is given in Fig. 7.

Time required on Atlas for this program is approximately two minutes, the main proportion of which is consumed by storage. Only two seconds is required to perform one pressure distribution.

6. Results and Discussion

6.1 Example 1 - Tandem cascade

The tandem blade arrangement consists basically of a NACA 23012 profile with a particular slot arrangement which was found (Ref. 16, type 2-h) to be most satisfactory as a high-lift device for an isolated aerofoil. The unslotted main blade is designed with 20° camber and 12% thick. Full particulars of the first blade is shown in Fig. 13. Data of the 52 aerofoil points fed in the program are listed in Fig. 14.

To fill up the cut away portion, a 20C2/57.8P30 blade is used (Fig. 15).

Thus "flap" positions, one without and the other with 10 and 20° deflections, are used. The outlet angles are assumed to follow the camber line, i.e., without deviation. The stagger used in this example is 40°.

Figs. 4, 5 and 6 show the results from first, second and final transformation. Fig. 16 listed the first 30 terms of the 100 Fourier coefficients

after/

after the third iteration. It can be seen from Fig. 17 that there is little difference in ϵ between the results after the third and the fourth iteration. It was therefore decided that three iterations should be used throughout.

In order to prove that the Fourier coefficients are sufficiently accurate, they are used to recalculate the value of ψ (ae^{ψ_0} is the radius of true circle) which should be constant for all aerofoil points. As shown in Fig. 18, the errors involved are between - 0·1275% and + 0·1125%. In most cases, they are within ± 0·05% accurate.

In Fig. 12, it has been shown that the curve fitting program manages extremely well. A further check on its results can be obtained from the curve $|d\zeta/dz|$ overall in Fig. 19.

As explained in the previous section, only the circulation effect is included in this report. Fig. 20 shows the pressure distribution curves for three positions of the second blade: (a) without second blade effect, (b) position equivalent to 10° deflection, and (c) position equivalent to 20° deflection. As can be seen, the areas under the curves increase considerably with the effect of increasing circulation. This effect produced by the second blade is as expected.

The curves, however, exhibit a somewhat unexpected undulation. Its unsmoothness is more pronounced on the suction surface. Further investigation shows this feature is rather 'natural' though it may not be so pronounced in reality.

The variation of the velocity on the circle in the final transformation is governed by a set of singularities. A typical velocity curve for a circle with such effects is plotted in Fig. 21. Assuming the trailing edge is at $\theta = 0°$ and the leading edge is at 190°, the velocity curve belongs to a fourth order polynomial. In the same graph, a typical $d\zeta/dz$ curve (of the third order type) is also plotted. Since the product of these two curves is the final velocity, this resultant must be of a seventh order polynomial curve.

Another extraordinary feature of this resultant velocity curve is that it is extremely sensitive to errors in the $d\zeta/dz$ curve. Figs. 22 and 23 show the basic calculation by two different methods. The former uses 100 terms of Fourier series and exact $d\zeta/dz$ method as described in the previous section. The latter employs only 10 terms of Fourier coefficients and a general five point, fourth order curve fitting process for $d\zeta/dz$. These curves in both figures look extremely close with only 1 to 2% difference at some points, yet the V/V_1 curves wave in opposite directions. The two V/V_1 curves are shown superimposed in Fig. 22.

6.2 Example 2

This example shows a comparison of the present method and the experimental results from Carter and Hughes[2] of the profile 11C2/33P40. Instead of using 12 points as in that report, 46 points are employed. One hundred terms of Fourier coefficients are used.

Fig. 24 shows the pressure distribution round the profile. The same characteristic, i.e., very rugged curve, again exists.

Two/

Two interesting results are observed from this calculation. For 100 terms of Fourier series, the first 30 terms converge very rapidly. Within 30 terms, the magnitude is reduced to about 100th of the largest term. The other feature is that the assumption of $\theta_1 \simeq \phi_1$ is found to be very fair (at least for this profile). The values between the first and the second iteration are within 0·2° and the second and third within 0·03°.

The results obtained compare favourably on the suction surface but not on the pressure surface. The difference between the deviation is nearly 2° between the theoretical and experimental values.

6.3 Conclusion

The method developed in this report would seem to be the best way to perform the Howell method and the Theodorsen transformation satisfactorily, especially with irregular profiles. The advantages are that it does not require any form of interpolation and that it is fully automatic.

7. Notation

A_n, B_n	Fourier coefficients
A'_n, B'_n	Fourier coefficients
a, a_1	see Fig. 3; also in the expression ae^{ψ_o}
c	modulus of $(a^2 e^{-i\alpha_1} - a_1 e^{i\alpha_1})$
c_2, c_3	constants for Joukowski transformation
C_a	axial velocity
f	see equation (3.1)
g	see equation (3.1)
h	see equation (3.1)
i	$\sqrt{-1}$
j	see equation (3.1)
k	see equation (3.1)
k_1, $\bar{k}_1$	strength of doublet
K_2	circulation of second blade
ℓ	see equation (3.1)
m_1, m_2, m_3	ratio of radius of t_∞ and singularity points
r	radius of circle
t_1, t_2, t_{21}	tangent of air angles (inlet, outlet, inlet of second blade)
u	velocity in x-direction

v/

v	velocity in y-direction
V	local velocity
V_1	velocity at inlet
w	complex velocity in z-plane
W	complex potential function
Wu_1 , Wu_2	whirl velocity at inlet and outlet
x	co-ordinate in z-plane
y	co-ordinate in z-plane
α_1 , α_2	air inlet and outlet angle
α_{21}	air outlet angle of the first blade
β_1 , β_2 , β_3	relative angle of singularity (see Fig. 7)
Δ	$\lambda - \psi$
ϵ	$\phi - \theta$
λ	polar co-ordinate in z_4 plane, also direction of doublet (see Fig. 7)
ϕ	polar co-ordinate in z_4 plane, also velocity potential function
ψ	polar co-ordinate in ζ_4-plane, also stream function
θ	polar co-ordinate in ζ_4-plane
ζ	stagger, also transformed plane

Suffices

o	referring to points in z_4 plane
1	first transformation
2	second transformation
3	third transformation
4	fourth transformation

8. Acknowledgements

The authors wish to express their thanks to Prof. S. A. Tobias for the use of the facilities of the Department of Mechanical Engineering, and to the U.S. Army who supported the work.

References/

References

No.	Author(s)	Title, etc.
1	R. A. Brooker et al	The "Mercury Autocode Manual", 2nd Edition, List CS242A, Ferranti Ltd., June 1961.
2	A. D. S. Carter and Hazel P. Hughes	A theoretical investigation into the effect of profile shape on the performance of an aerofoil in a cascade. A.R.C. R.& M. 2384, March, 1946.
3	W. F. Durand (Editor)	Aerodynamic Theory, Vol. 2, 1935. Springer-Verlag, Berlin.
4	A. R. Howell	A theory of arbitrary aerofoil in cascade. Phil. Mag., Vol.37, 7th Series, 1948.
5	L. V. Kantroovich and V. I. Krylov	Approximate method of higher analysis. Translated by C. D. Benster, P. Noordhoff Ltd., Netherlands.
6	L. M. Milne-Thomson	Theoretical Aerodynamics. Macmillan and Co., London, 1948.
7	I. Naiman	Numerical evaluation of the ϵ-integral occurring in the Theodorsen arbitrary-airfoil potential theory. NACA ARR No.L4D27a, April 1944 (WR L-136).
8	I. Naiman	Numerical evaluation by harmonic analysis of the ϵ-function of the Theodorsen arbitrary-airfoil potential theory. NACA ARR No.L5H18, September 1945 (WR L-153).
9	H. Ohashi	Mutual interference in tandem compressor cascade. Bulletin J.S.M.E., Vol.7, No.25, 1964.
10	D. Pollard and J. Wordsworth	A comparison of two methods for predicting the potential flow around arbitrary airfoils in cascade. A.R.C. C.P.618, June 1962.
11	J. W. Railly and E. Elsahra	Ackeret's method for tandem cascade. Research Report No.Mech.Eng. Dept. Birmingham University 1964.
12	W. E. Spraglin	Flow through cascades in tandem. NACA TN 2393, June 1951.
13	T. Theodorsen	Theory of wing sections of arbitrary shape. NACA Report No.411, 1931.
14	B. Thwaites	On the numerical calculation of Theodorsen's transformation. A.R.C. C.P.691, January 1963.

No.	Author(s)	Title, etc.
15	E. J. Watson	Formulae for the computation of the functions employed for calculating the velocity distribution about a given aerofoil. A.R.C. R.& M. 2176, May 1945.
16	C. J. Wenzinger and T. A. Harris	Wind-tunnel investigation of an N.A.C.A.23012 airfoil with various arrangements of slotted flaps. NACA Report No. 664, 1939.

ES

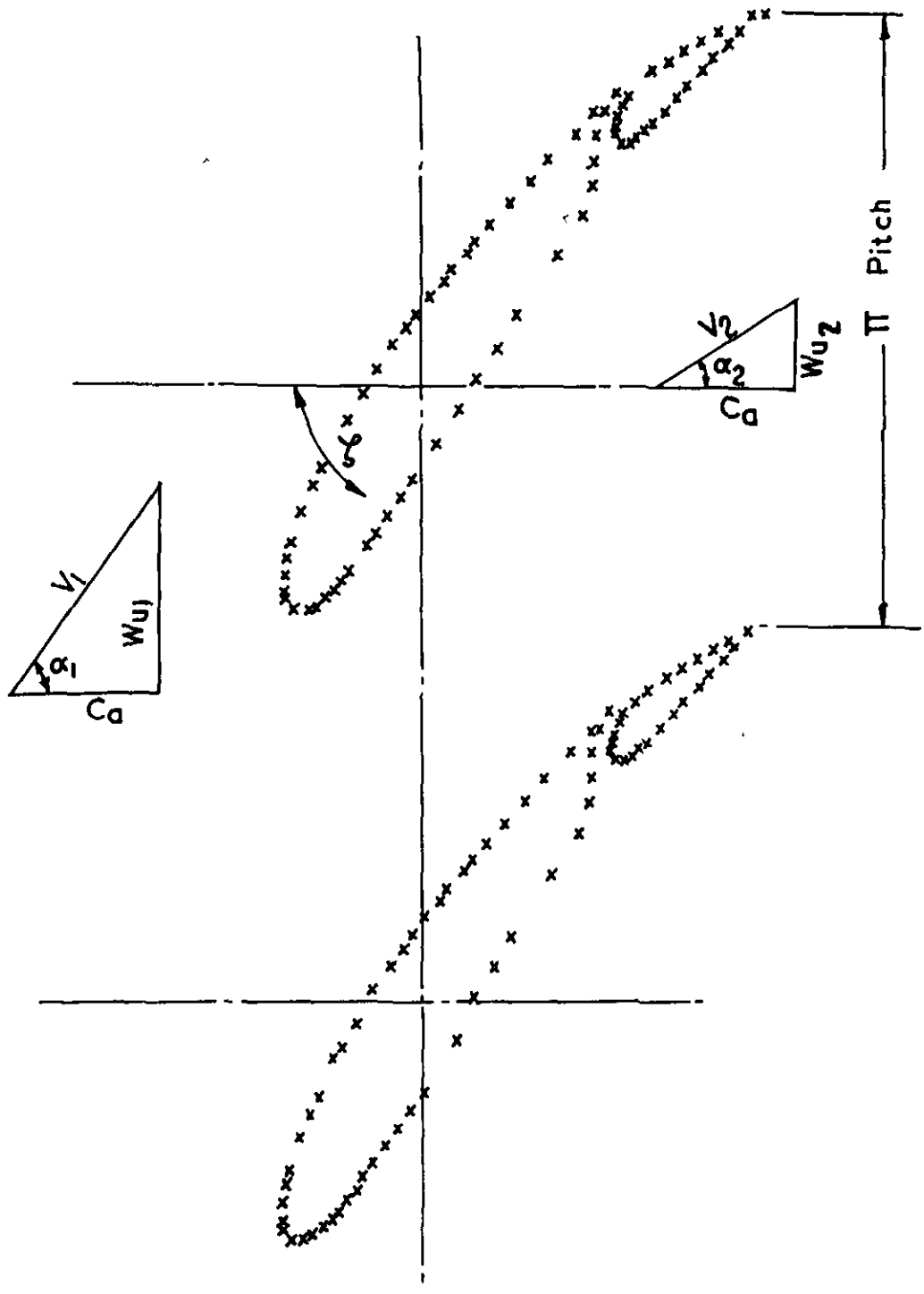

FIG. 1 Cascade geometry

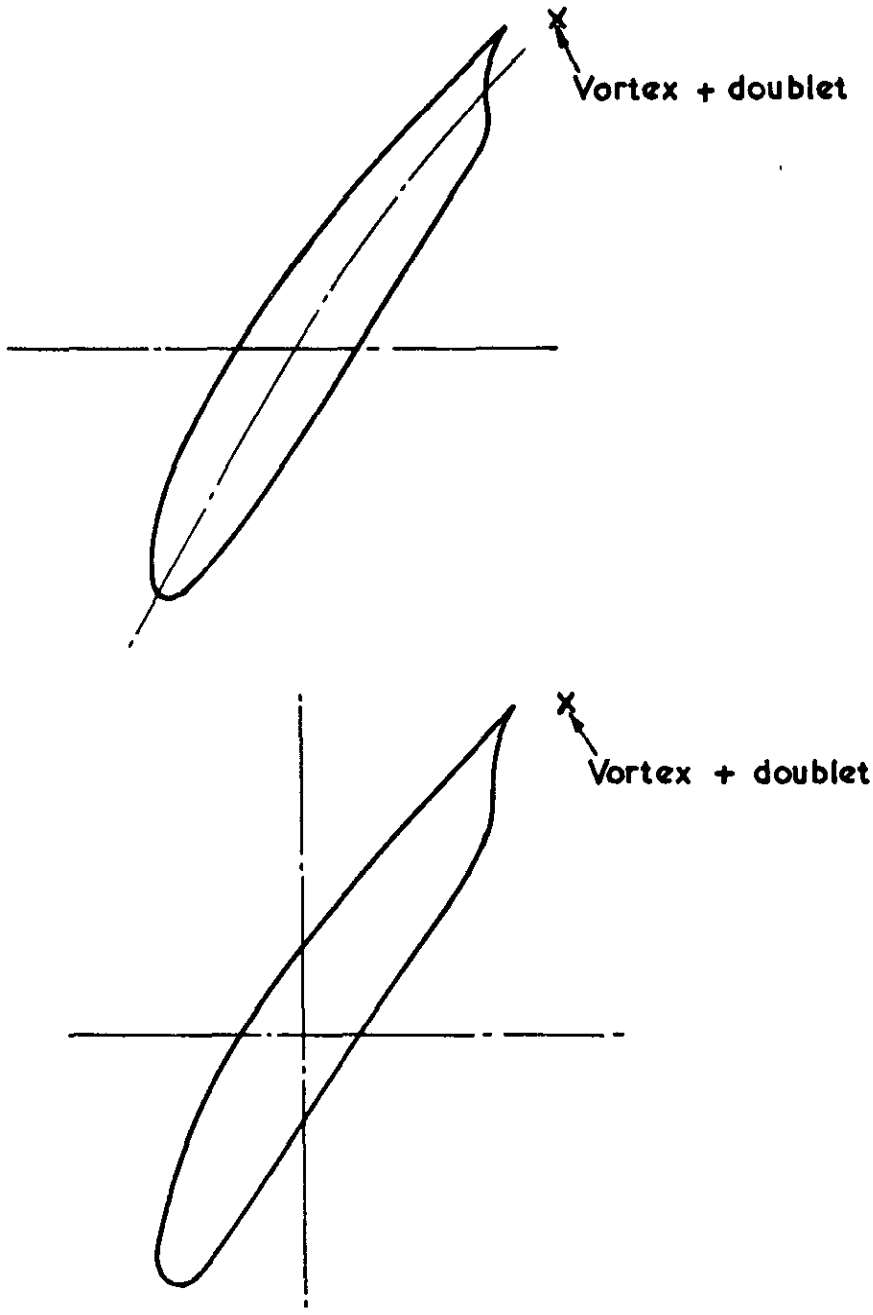

FIG. 2 Equivalent cascade

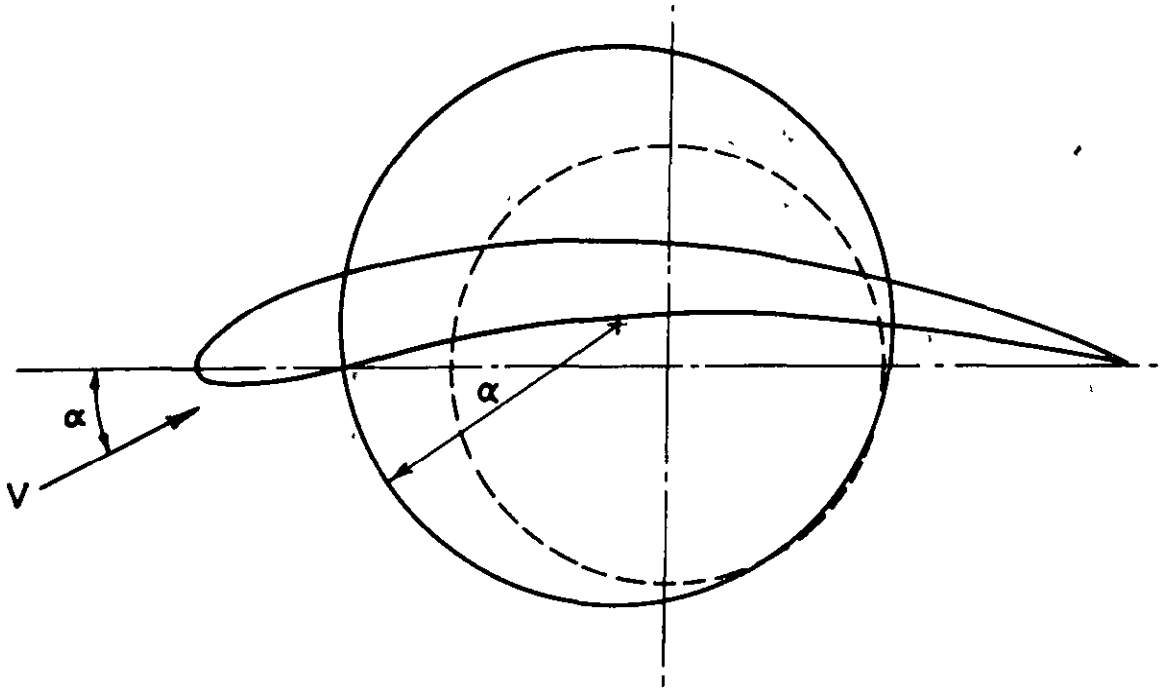

a = radius of circle

a_1 = 0·25 chord length approx.

Strength of doublet = $V[a^2 e^{-i\alpha} - a_1 e^{i\alpha}]$

FIG. 3 Substitutional singularity

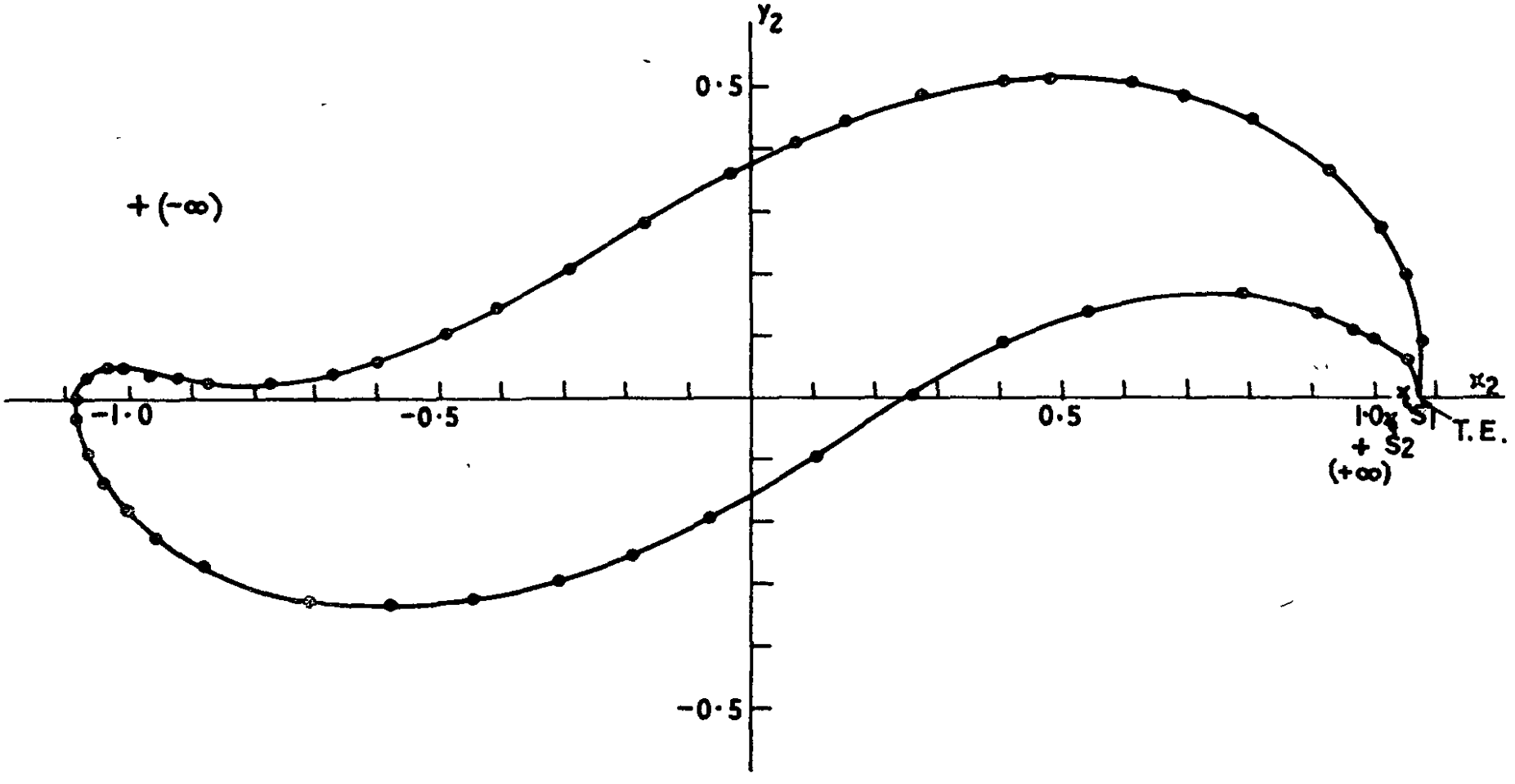

FIG. 4. First transformation, $\zeta = 40^0$

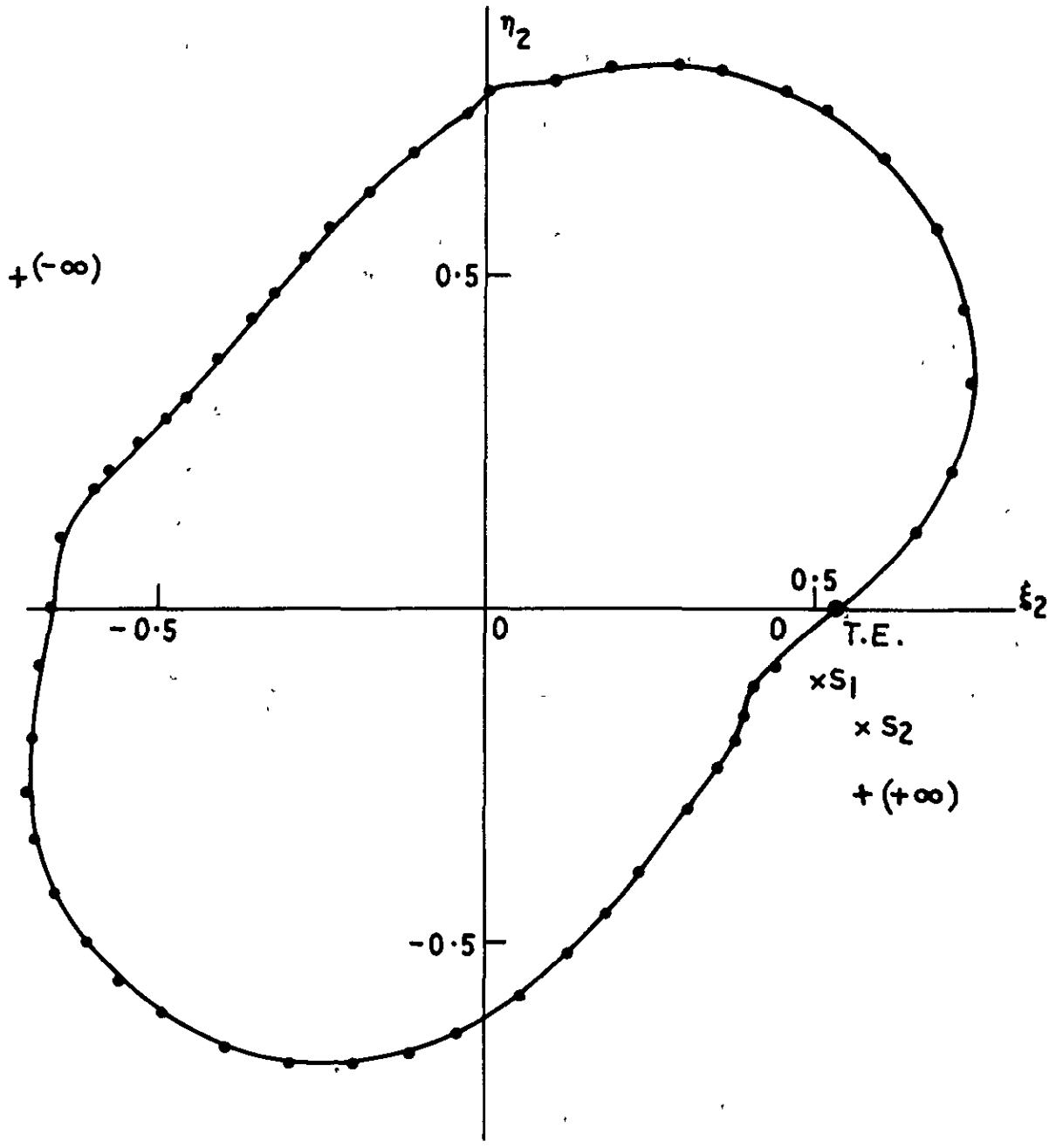

FIG. 5 2nd transformation, $\zeta = 40°$

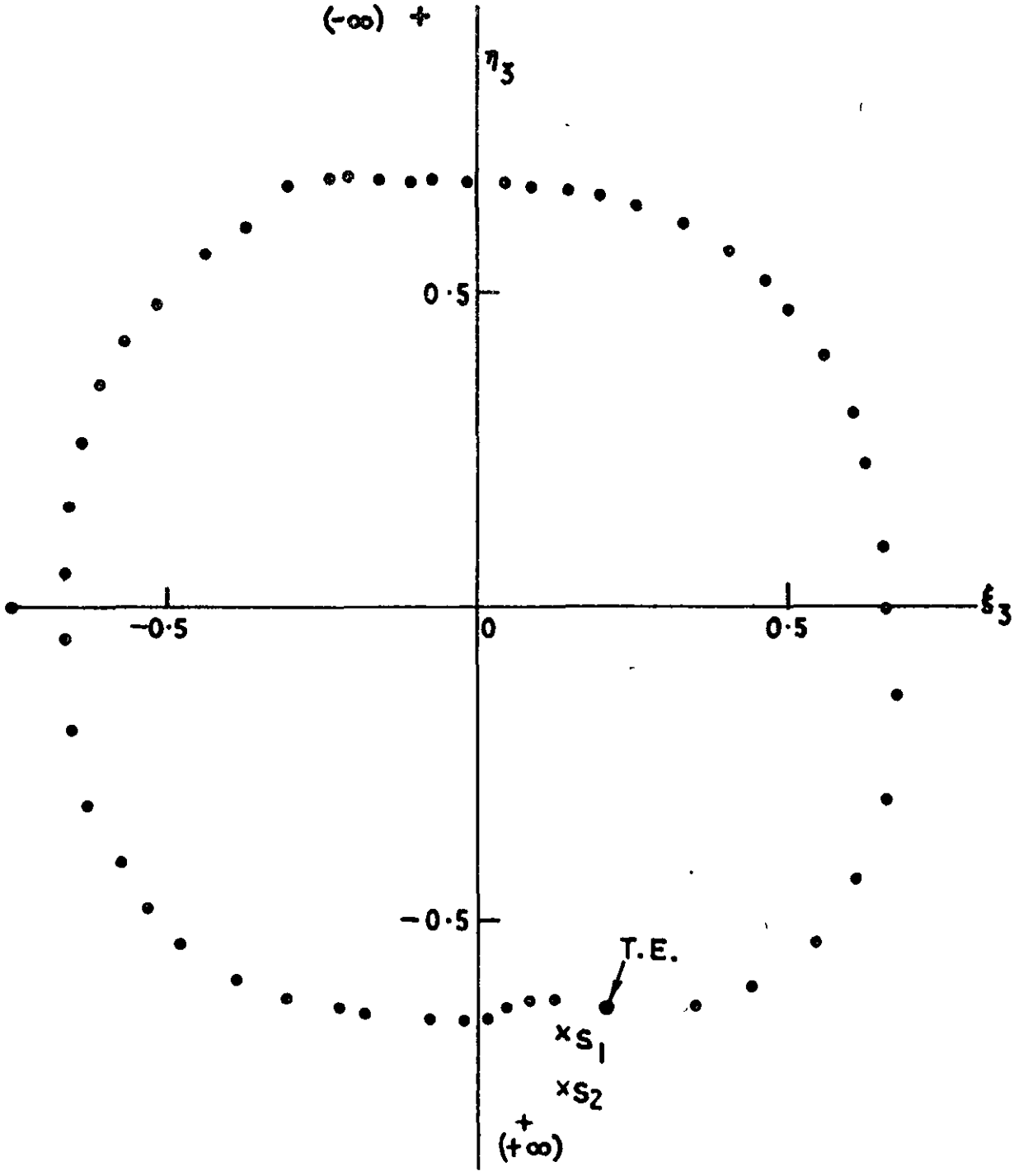

FIG. 6 3rd transformation, $\ell = 40^0$

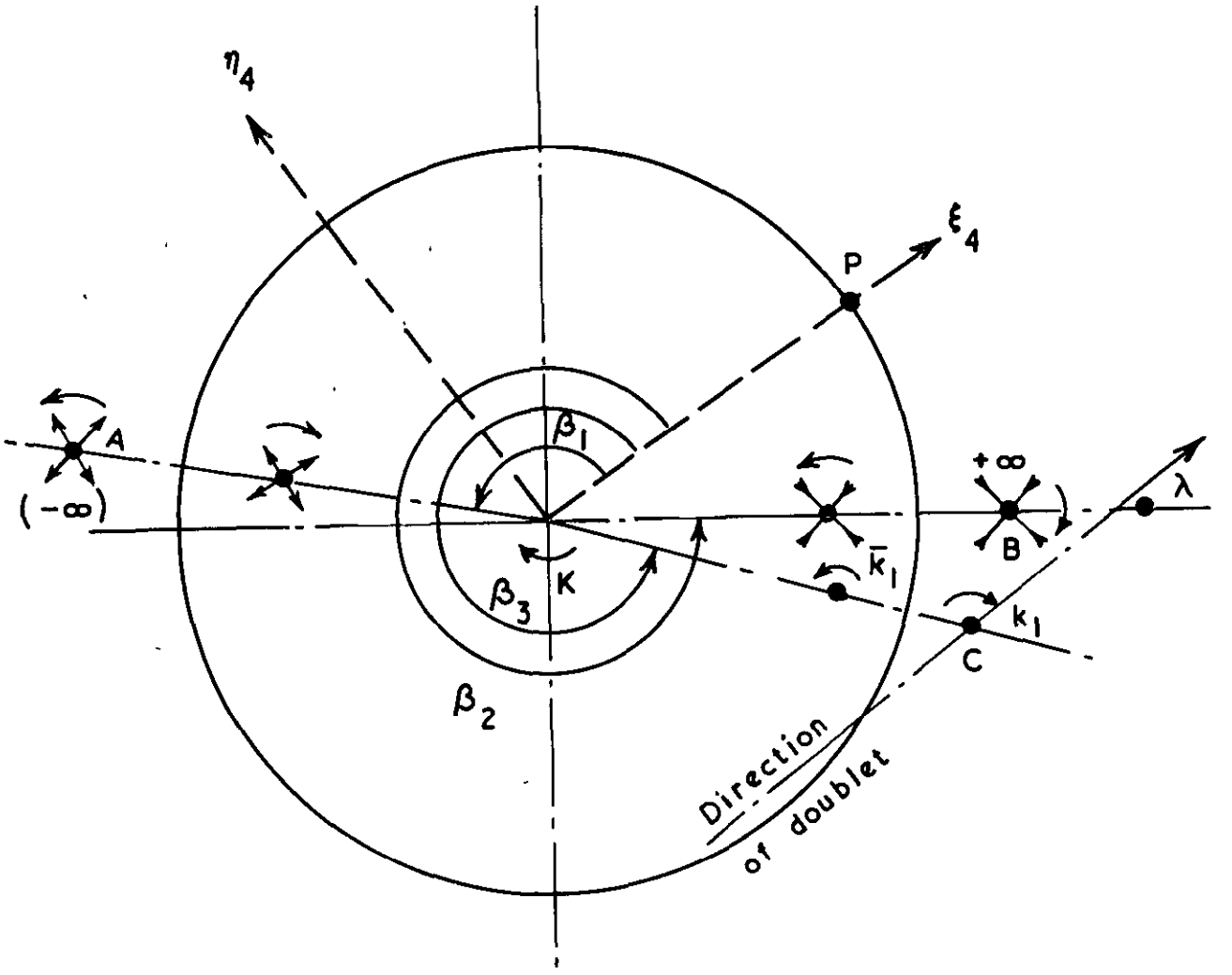

Key

Source and sink

Vortex

FIG. 7 Flow in circle ζ_4 plane

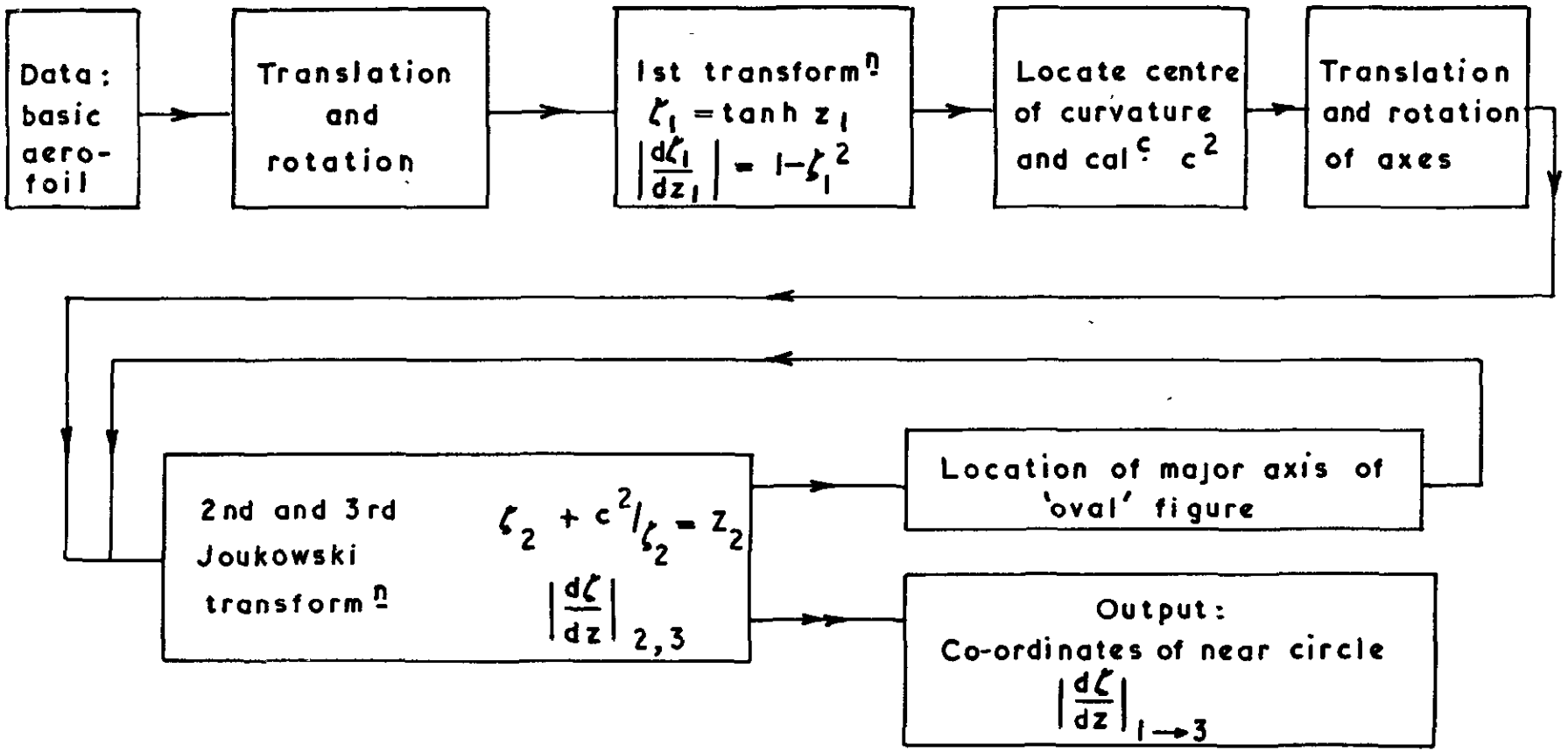

FIG. 8 Block diagram for program 1

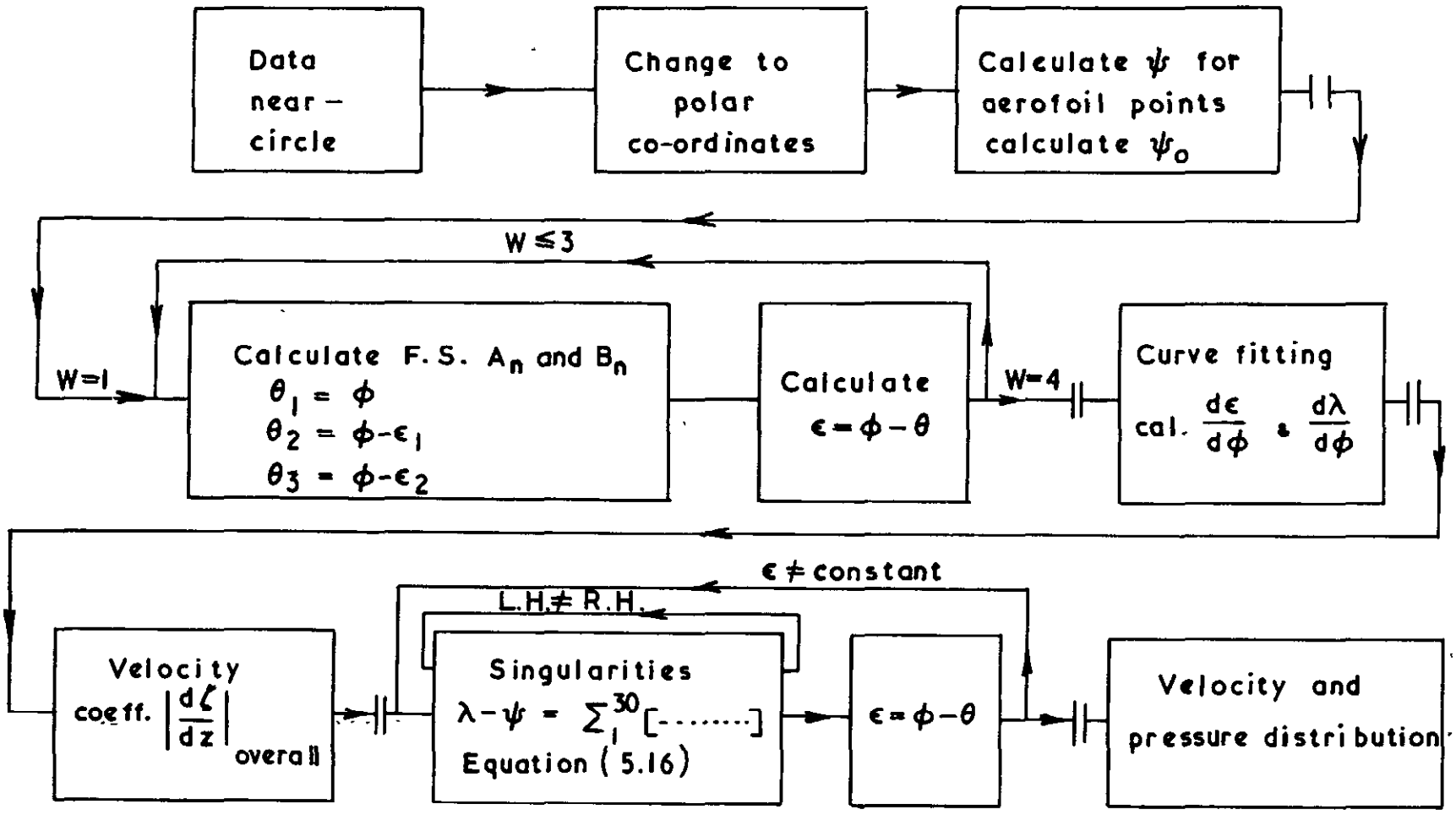

⊣⊢ New chapter

FIG 9 Block diagram for program 2

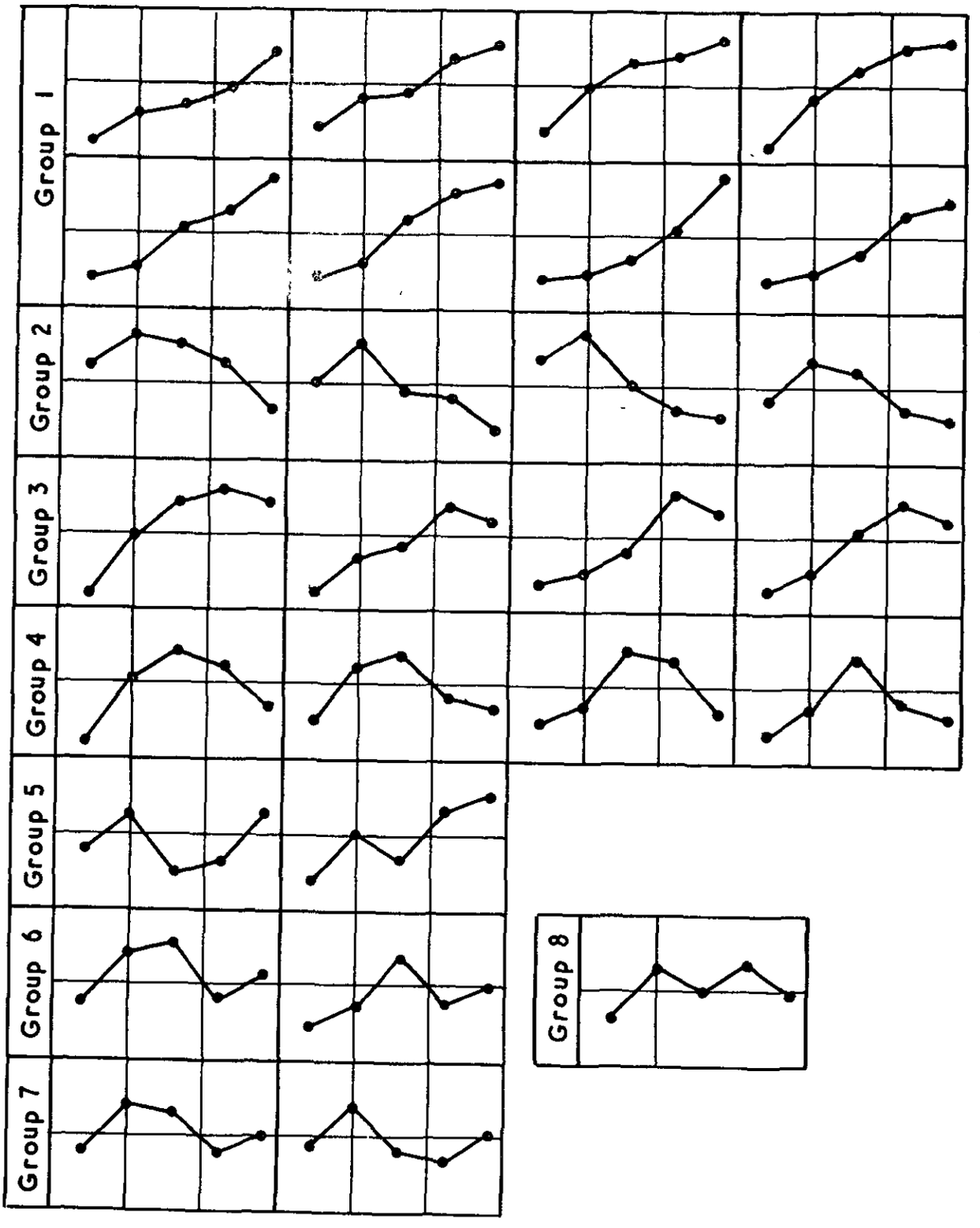

FIG. 10 Possible path of curves through 5 points

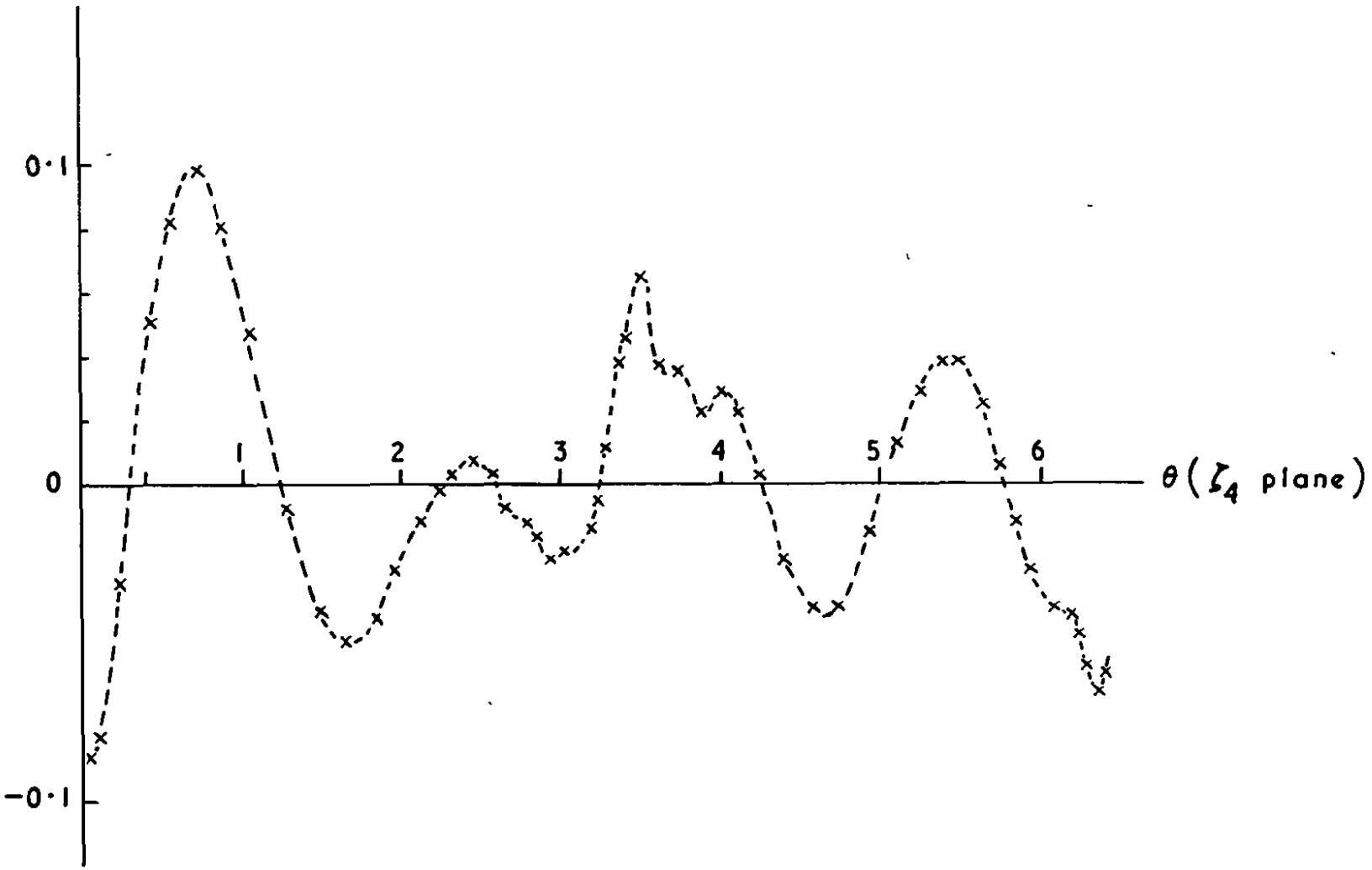

FIG. 11 Typical λ v. θ curve

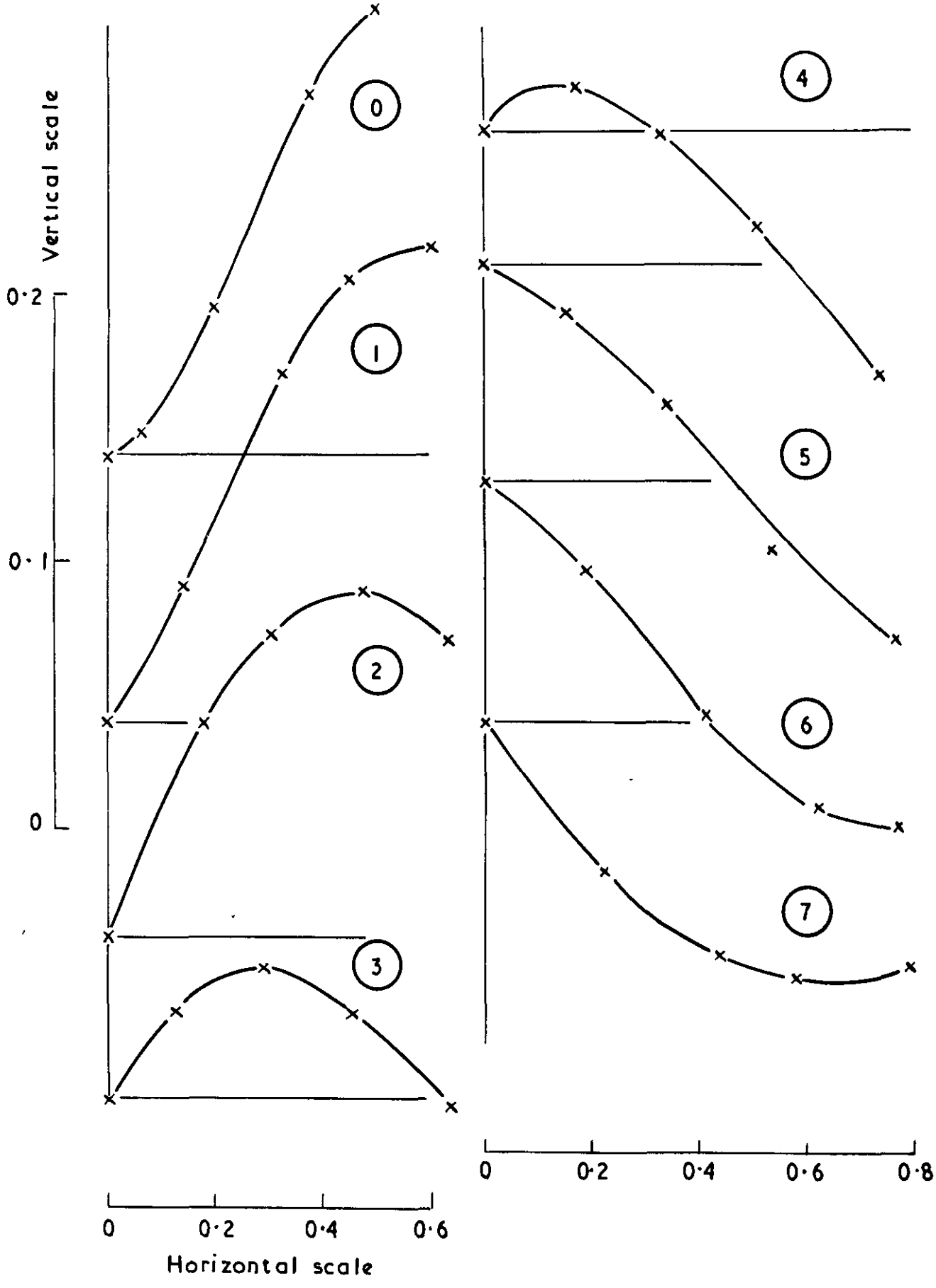

FIG. 12 A Examples of curve fitting program

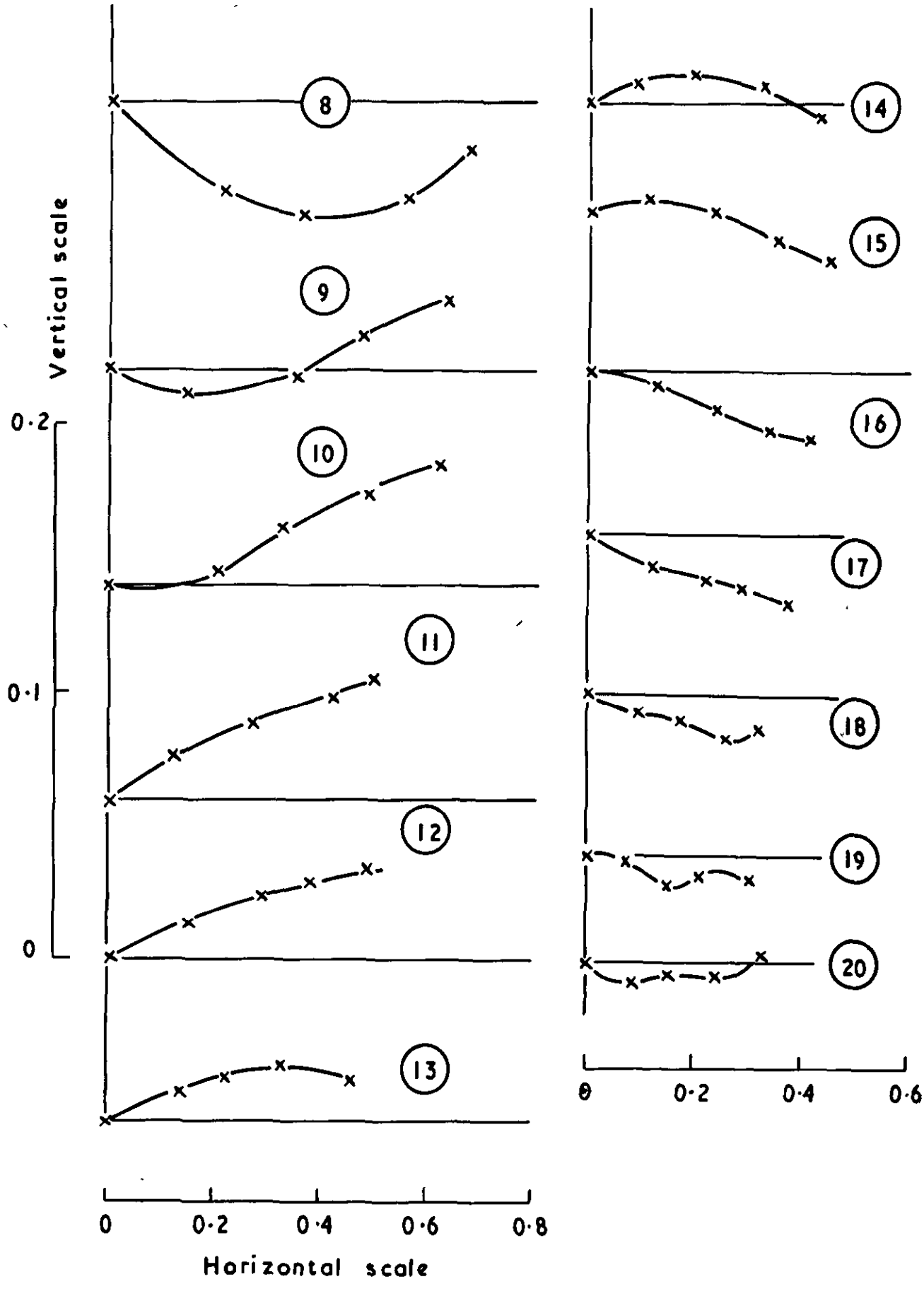

FIG. 12 B Examples of curve fitting program

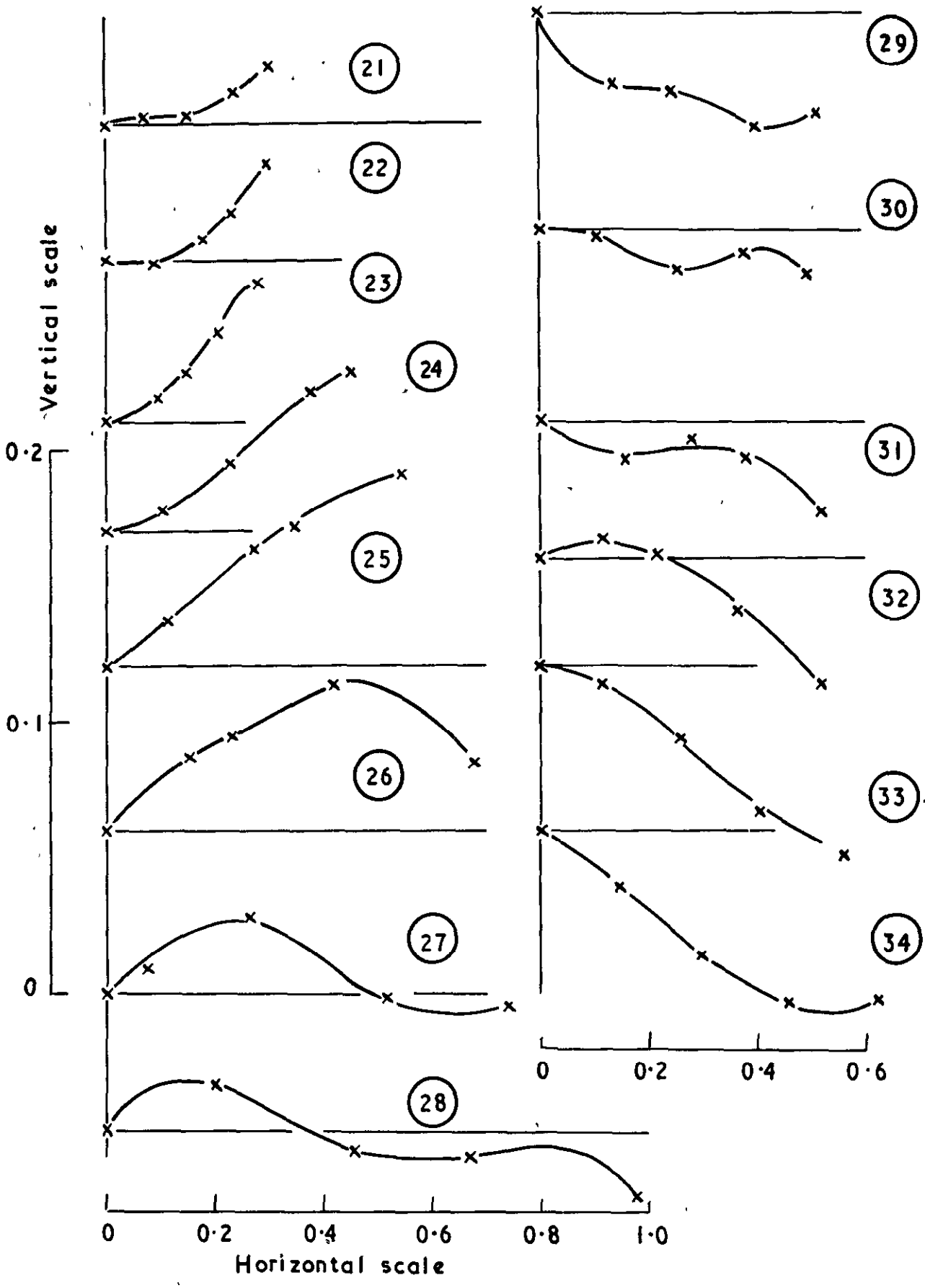

FIG. 12C Example of curve fitting program

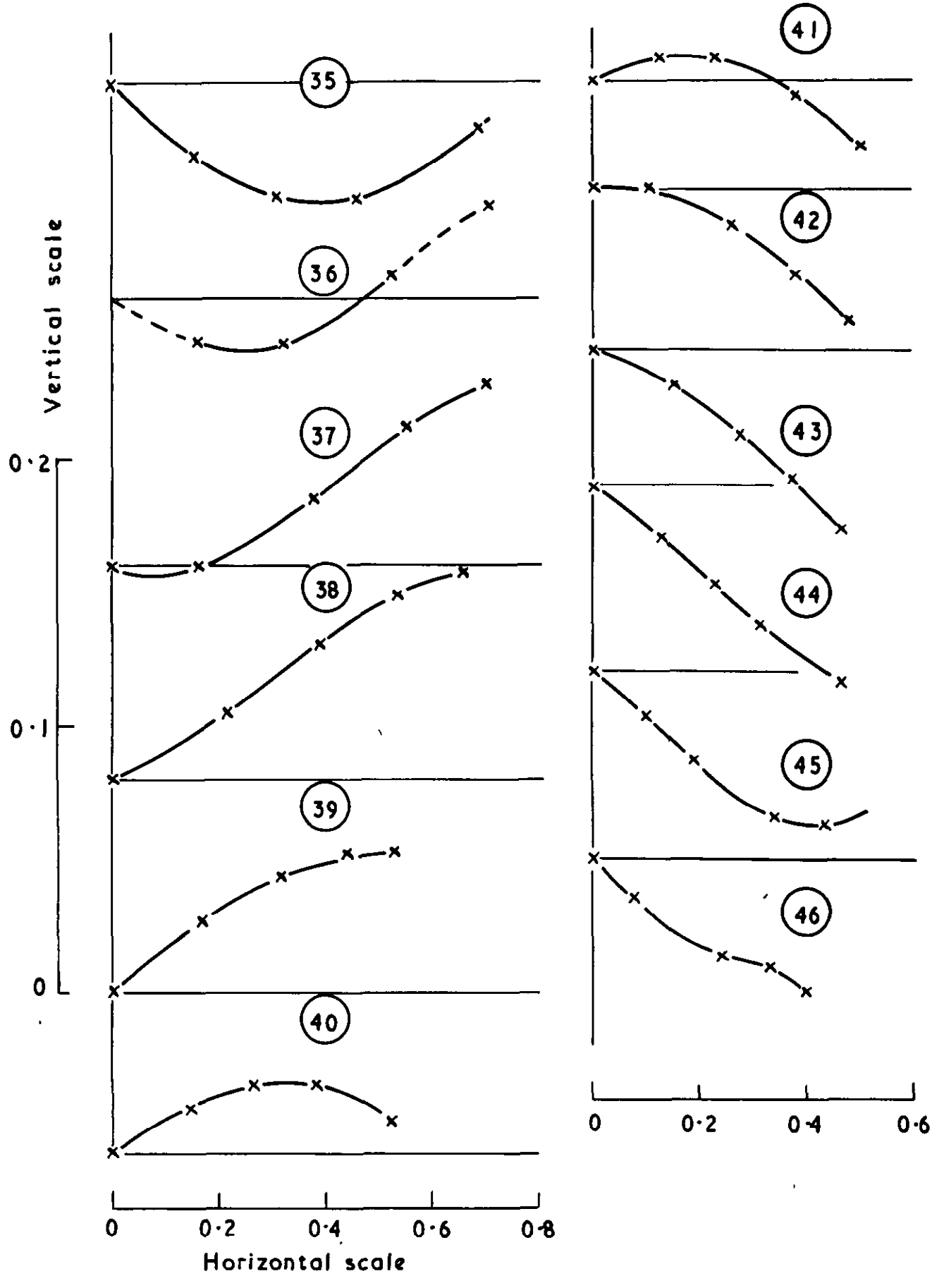

FIG. 12D Example of curve fitting program

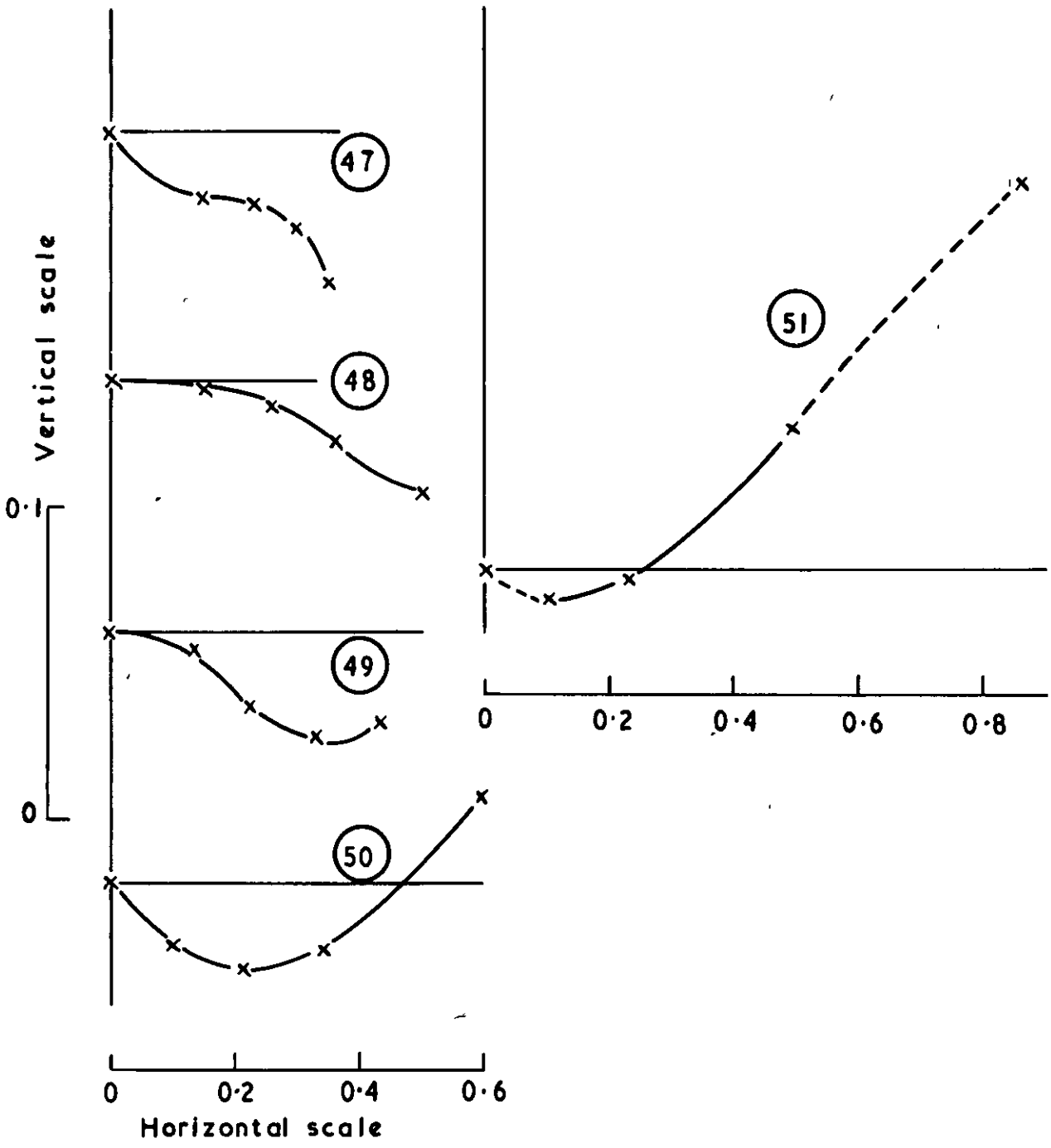

FIG. 12 E Examples of curve fitting program

x/c	0	0·01	0·02	0·04	0·07	0·10	0·15	0·20	0·25	0·30	0·40	0·50	0·60	0·70	0·80	0·90	0·95	1·00
y/c upper	0	0·026	0·034	0·046	0·058	0·069	0·080	0·088	0·092	0·094	0·096	0·092	0·081	0·069	0·050	0·029	0·016	0
y/c lower	0	$\bar{0}$·013	$\bar{0}$·019	$\bar{0}$·023	$\bar{0}$·029	$\bar{0}$·030	$\bar{0}$·030	$\bar{0}$·0295	$\bar{0}$·029	$\bar{0}$·028	$\bar{0}$·023	$\bar{0}$·018	$\bar{0}$·013	$\bar{0}$·010	$\bar{0}$·006	$\bar{0}$·002	$\bar{0}$·001	0

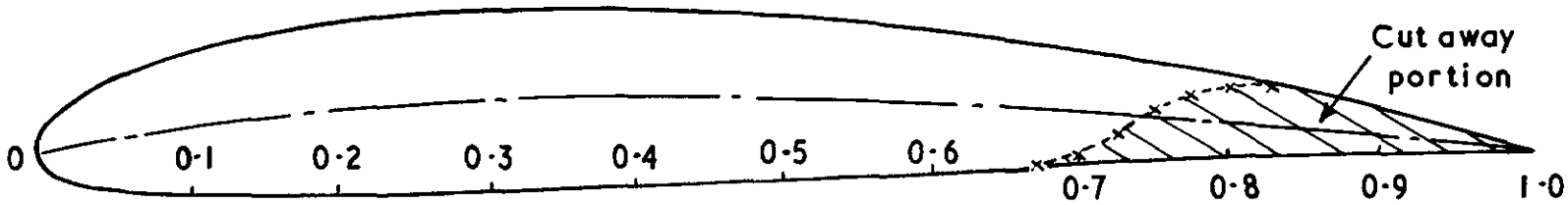

Basic profile : 23012

Camber : parabolic arc 20°

L.E. angle : 13° 56′

T.E. angle : 6° 4′

Max. thickness : 12% chord

FIG. 13 First blade (basic)

Position	x	y	Position	x	y	Position	x	y
0	0·828	0 044	20	0·150	0 080	40	0·270	-0·029
1	0·790	0·052	21	0·110	0·070	41	0 300	-0·028
2	0·750	0·060	22	0·070	0·058	42	0·350	-0·025
3	0·700	0·069	23	0·050	0·050	43	0·400	-0·022
4	0·660	0·073	24	0·030	0·040	44	0·450	-0·020
5	0·620	0·079	25	0·010	0·026	45	0·500	-0·018
6	0·580	0·084	26	0·005	0·018	46	0·600	-0·014
7	0·550	0·088	27	0	0	47	0·665	-0·011
8	0·530	0·090	28	0·010	-0·013	48	0·710	-0·001
9	0·500	0·092	29	0·020	-0·019	49	0·740	0·022
10	0·480	0·094	30	0·040	-0·023	50	0·770	0·037
11	0·450	0·095	31	0·055	-0·027	51	0·800	0·044
12	0·420	0·096	32	0·070	-0·029	52		
13	0·400	0·097	33	0·090	-0·030			
14	0·370	0·098	34	0·110	-0·030			
15	0·330	0·097	35	0·130	-0·030			
16	0·290	0·094	36	0·150	-0·030			
17	0·250	0·092	37	0·180	-0·030			
18	0·220	0·090	38	0·210	-0·030			
19	0·180	0·083	39	0·240	-0 0295			

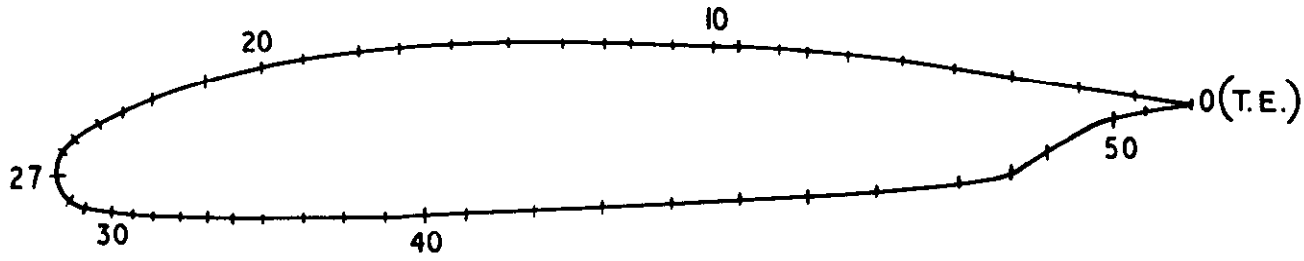

FIG. 14 First blade data for computer program

x	y_{upper}	y_{lower}
0	0·056	0
0·02	0·082	-0·016
0·04	0·100	-0·022
0·08	0·122	-0·032
0·14	0·144	-0·036
0·20	0·156	-0·040
0·30	0·160	-0·040
0·40	0·156	-0·036
0·50	0·140	-0·032
0·60	0·120	-0·028
0·70	0·096	-0·024
0·80	0·068	-0·020
0·90	0·036	-0·008
1·00	0	0

Camber: 57·8°
L.E. angle: 50·2°
T.E. angle: 7·6°
Max thickness: 30% chord

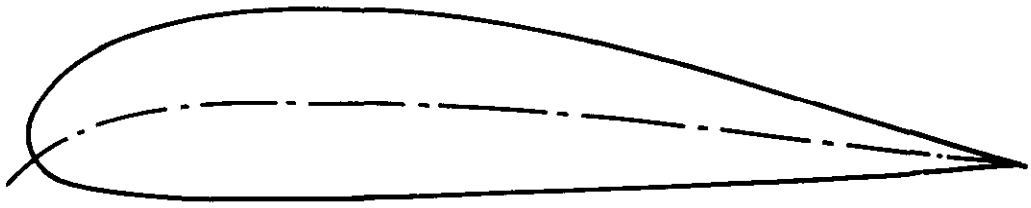

20C2/57·8 P30

FIG.15 Second blade

n	A'_n	B'_n
1	0.0057849704	0.0021347040
2	0.0076996322	0.0254522575
3	-0.0251959583	0.0050308940
4	-0.0375511861	0.0124040633
5	-0.0068147800	-0.0025866940
6	-0.0030278501	0.0060191149
7	-0.0043790720	-0.0049646100
8	-0.0070671758	0.0035498759
9	0.0002784733	-0.0028036057
10	-0.0034384745	-0.0006371556
11	-0.0006769249	-0.0007448841
12	-0.0025005849	-0.0010656833
13	-0.0002919087	-0.0006284193
14	-0.0018351806	-0.0010906628
15	-0.0002823735	-0.0011130765
16	-0.0009054839	-0.0010493745
17	-0.0003307853	-0.0004044983
18	-0.0005118550	-0.0009114503
19	-0.0008279345	-0.0001602631
20	-0.0003782335	-0.0003957844
21	-0.0008702815	-0.0006867121
22	-0.0003036657	-0.0001593109
23	-0.0004989425	-0.0006612783
24	-0.0010186003	-0.0001376830
25	-0.0000320395	-0.0005206492
26	-0.0007032967	-0.0004264968
27	-0.0001070366	-0.0000228661
28	-0.0006918023	-0.0003476893
29	-0.0002231776	0.0000613803
30	-0.0005283679	-0.0002304318

FIGURE 16 FIRST 30 TERMS OF FOURIER COEFFICIENTS AFTER 3rd ITERATION (From Program 6/7-4)

Position	3rd Iterat^{n}	4th Iterat^{n}	Position	3rd Iterat^{n}	4th Iterat^{n}	Position	3rd Iterat^{n}	4th Iterat^{n}
0	.0980	.0979	20	.0203	.0203	40	.0088	.0088
1	.0191	.0191	21	.0313	.0313	41	-.0087	-.0086
2	.0561	.0559	22	.0454	.0454	42	-.0282	-.0281
3	.0019	.0019	23	.0532	.0532	43	-.0372	-.0370
4	-.0415	-.0416	24	.0585	.0585	44	-.0382	-.0380
5	-.0715	-.0715	25	.0519	.0519	45	-.0331	-.0329
6	-.0750	-.0751	26	.0425	.0425	46	-.0137	-.0133
7	-.0512	-.0513	27	.0114	.0113	47	-.0014	-.0007
8	-.0271	-.0271	28	-.0121	-.0121	48	.0032	.0042
9	.0032	.0032	29	-.0149	-.0149	49	.0131	.0145
10	.0144	.0143	30	-.0175	-.0175	50	.0349	.0360
11	.0174	.0174	31	-.0210	-.0210	51	.0634	.0632
12	.0169	.0169	32	-.0332	-.0332			
13	.0139	.0139	33	-.0420	-.0420			
14	.0060	.0060	34	-.0356	-.0355			
15	-.0032	-.0032	35	-.0146	-.0146			
16	-.0046	-.0046	36	.0117	.0117			
17	-.0001	-.0001	37	.0346	.0347			
18	.0035	.0034	38	.0359	.0360			
19	.0125	.0124	39	.0247	.0248			

FIGURE 17 COMPARISON OF ε BETWEEN 3rd AND 4th ITERATION

(Results from Program 6/7-4)

Position	e^{Ψ}	% error	Position	e^{Ψ}	% error
0	1.0059	.0425	26	1.0056	.0125
1	1.0063	.0825	27	1.0066	.1125
2	1.0060	.0525	28	1.0051	-.0375
3	1.0060	.0525	29	1.0057	.0225
4	1.0057	.0225	30	1.0052	-.0275
5	1.0058	.0325	31	1.0059	.0425
6	1.0053	-.0175	32	1.0058	.0325
7	1.0051	-.0375	33	1.0057	.0225
8	1.0052	-.0275	34	1.0054	-.0075
9	1.0052	-.0275	35	1.0052	-.0275
10	1.0057	.0225	36	1.0051	-.0375
11	1.0056	.0175	37	1.0055	.0025
12	1.0055	.0025	38	1.0057	.0225
13	1.0057	.0225	39	1.0056	.0125
14	1.0058	.0325	40	1.0057	.0225
15	1.0057	.0225	41	1.0058	.0325
16	1.0055	.0025	42	1.0058	.0325
17	1.0054	-.0075	43	1.0057	.0225
18	1.0058	.0325	44	1.0058	.0325
19	1.0051	-.0375	45	1.0055	.0025
20	1.0057	.0225	46	1.0052	-.0275
21	1.0052	-.0275	47	1.0062	0.0725
22	1.0053	-.0175	48	1.0077	.1225
23	1.0051	-.0375	49	1.0069	.0925
24	1.0051	-.0375	50	1.0043	-.1175
25	1.0061	.0625	51	1.0042	-.1275

FIGURE 18

PERCENTAGE ERROR IN RADII (BLADE I) COMPARED WITH RADIUS OF TRUE CIRCLE (FROM PROGRAM 6/10-4.1)

$e^{\Psi_0} = 1.005475$

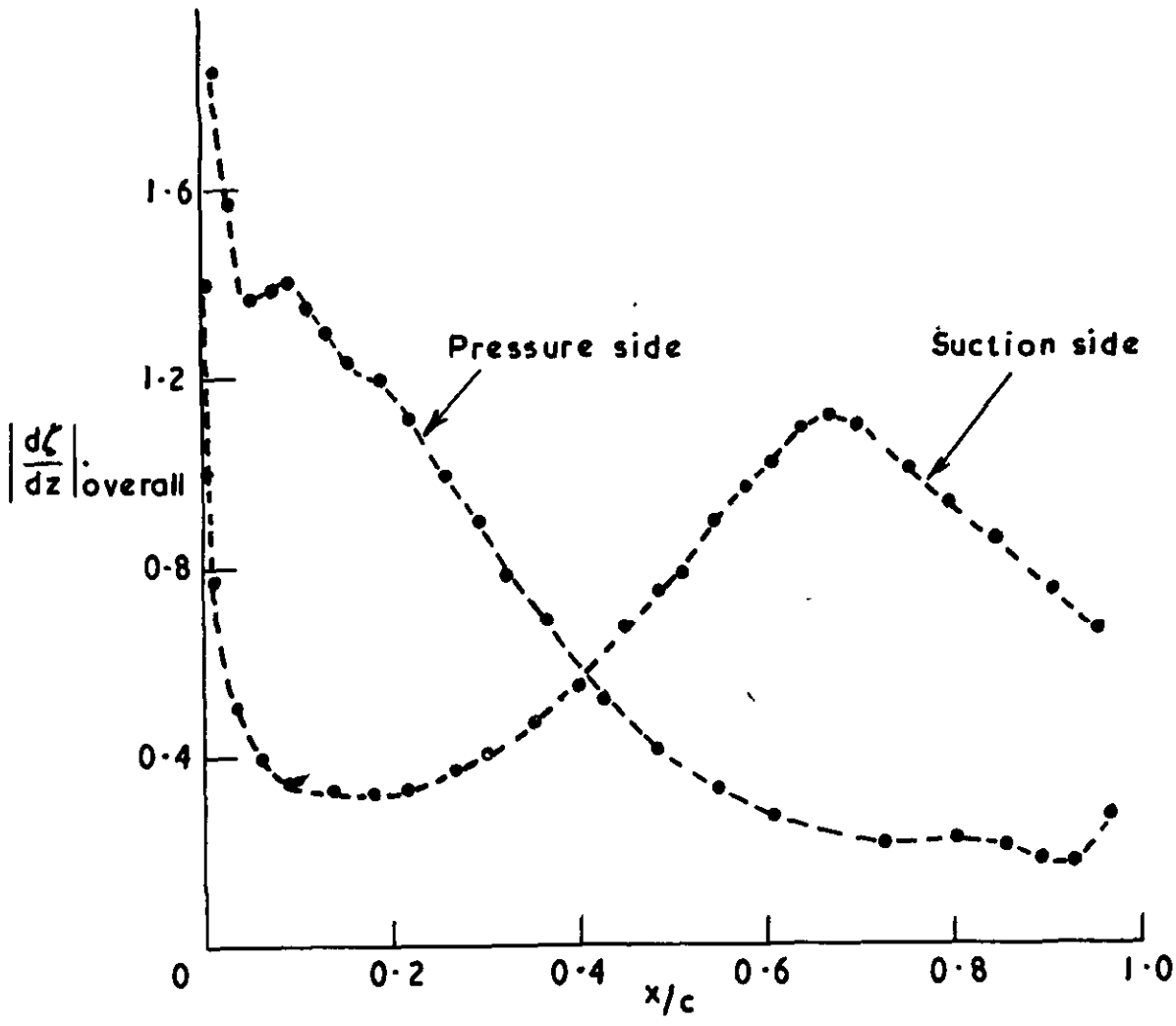

FIG. 19 — $\left|\frac{d\zeta}{dz}\right|$ for Example 1

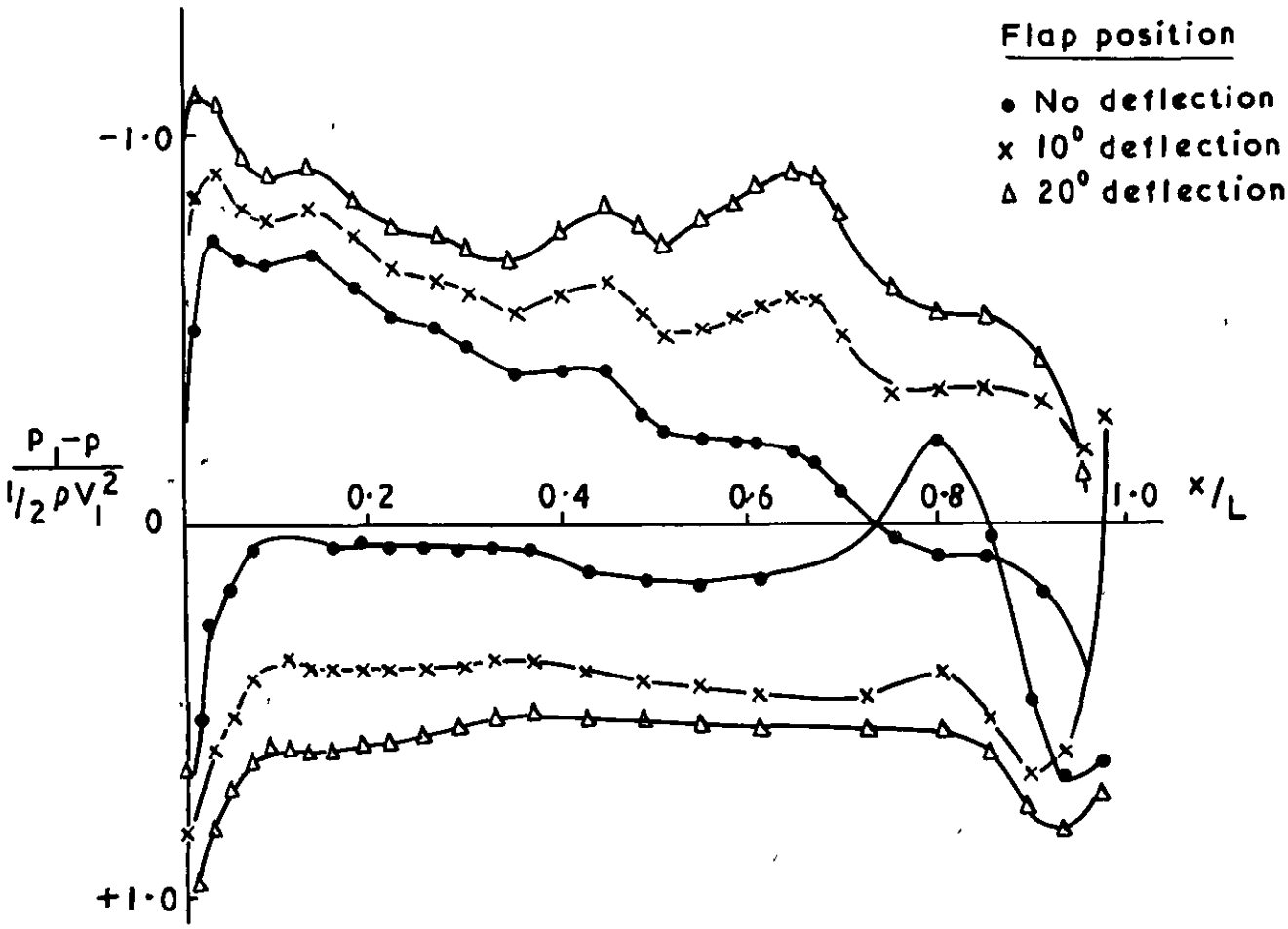

FIG. 20 Pressure distribution

$\zeta = 40^0$ $\alpha_l = 50^0$

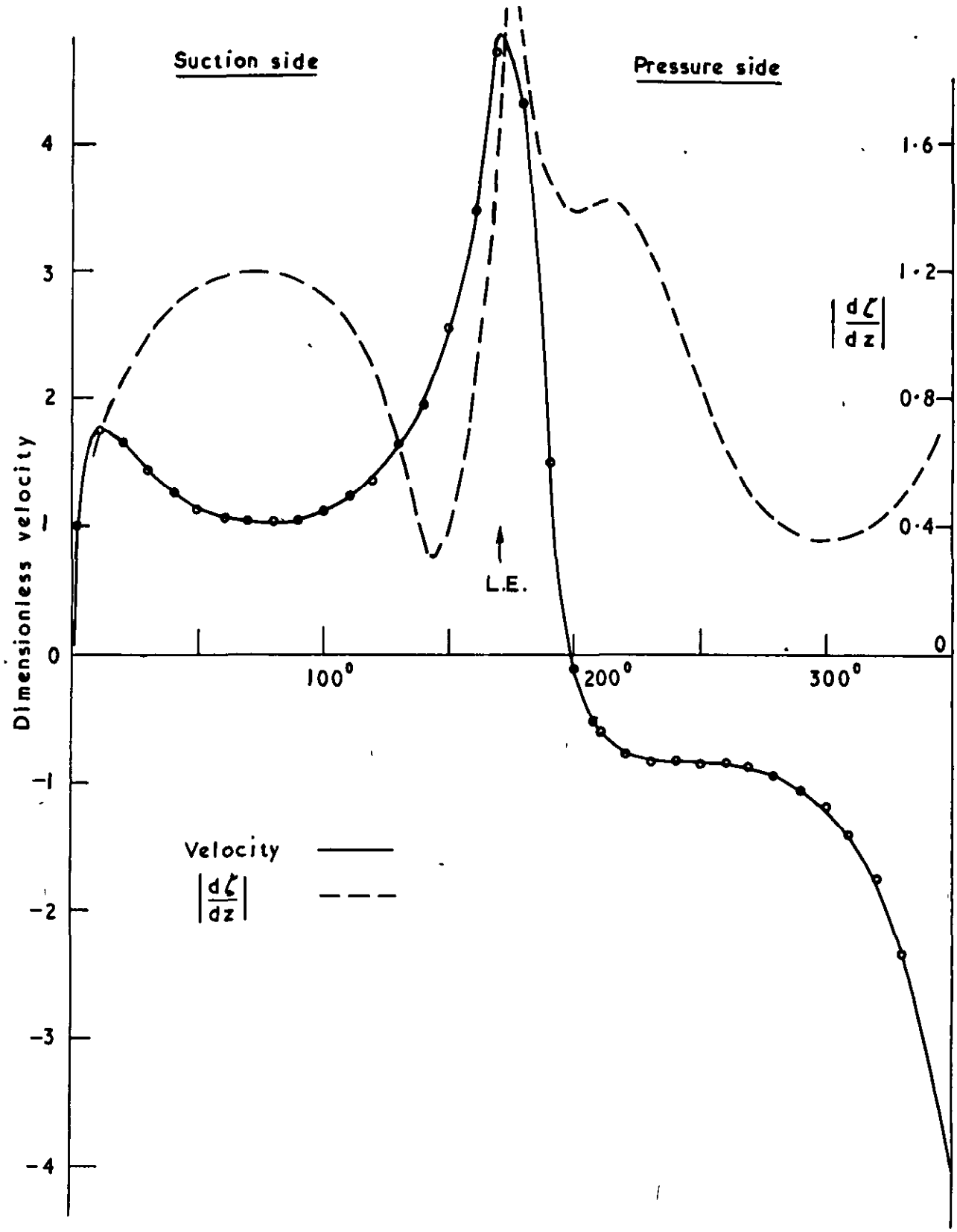

FIG. 21 Typical velocity and $\left|\frac{d\zeta}{dz}\right|$ curves in circle plane

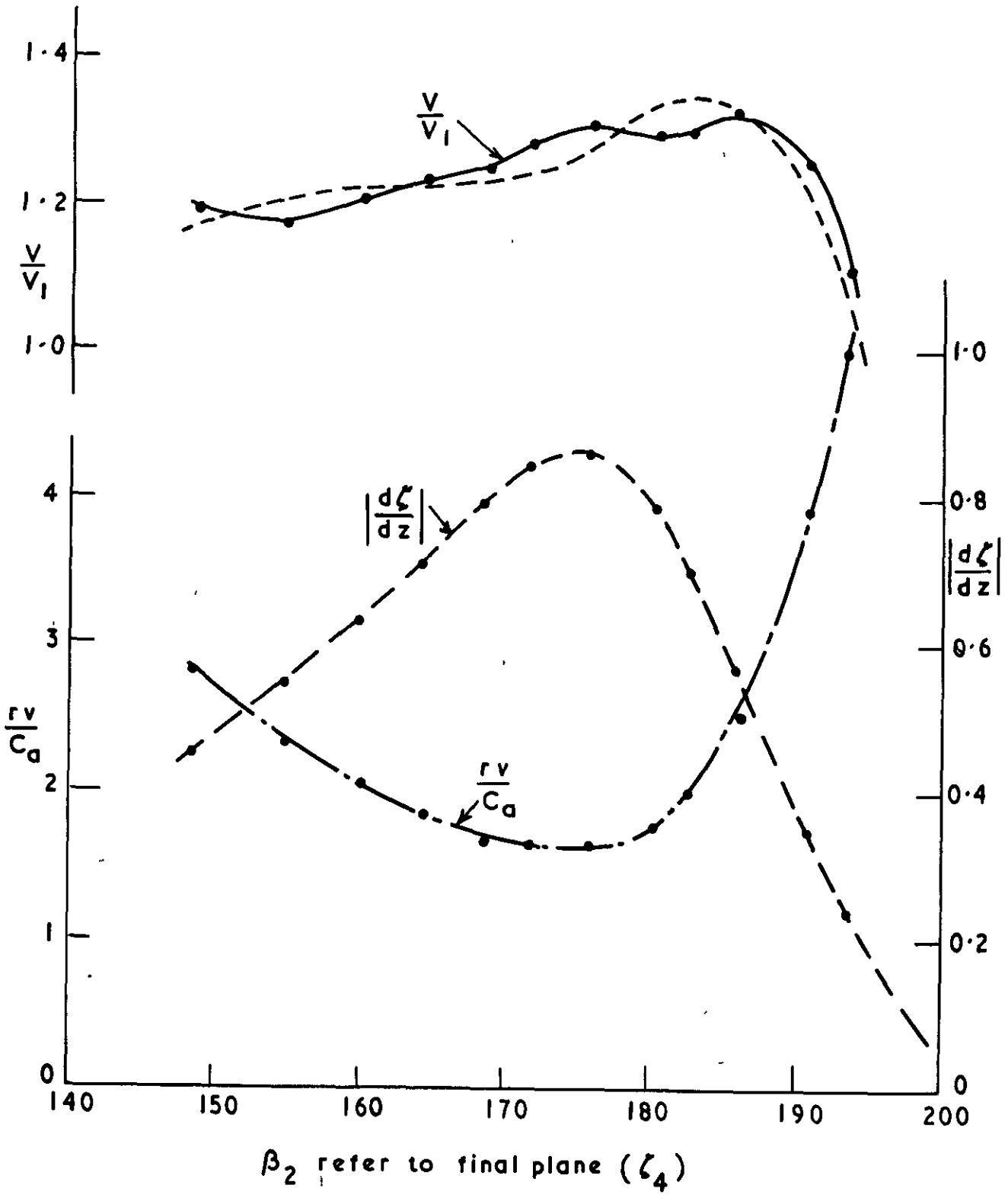

FIG. 22 Typical velocity curve near L.E. (Prog. 6/10-3)

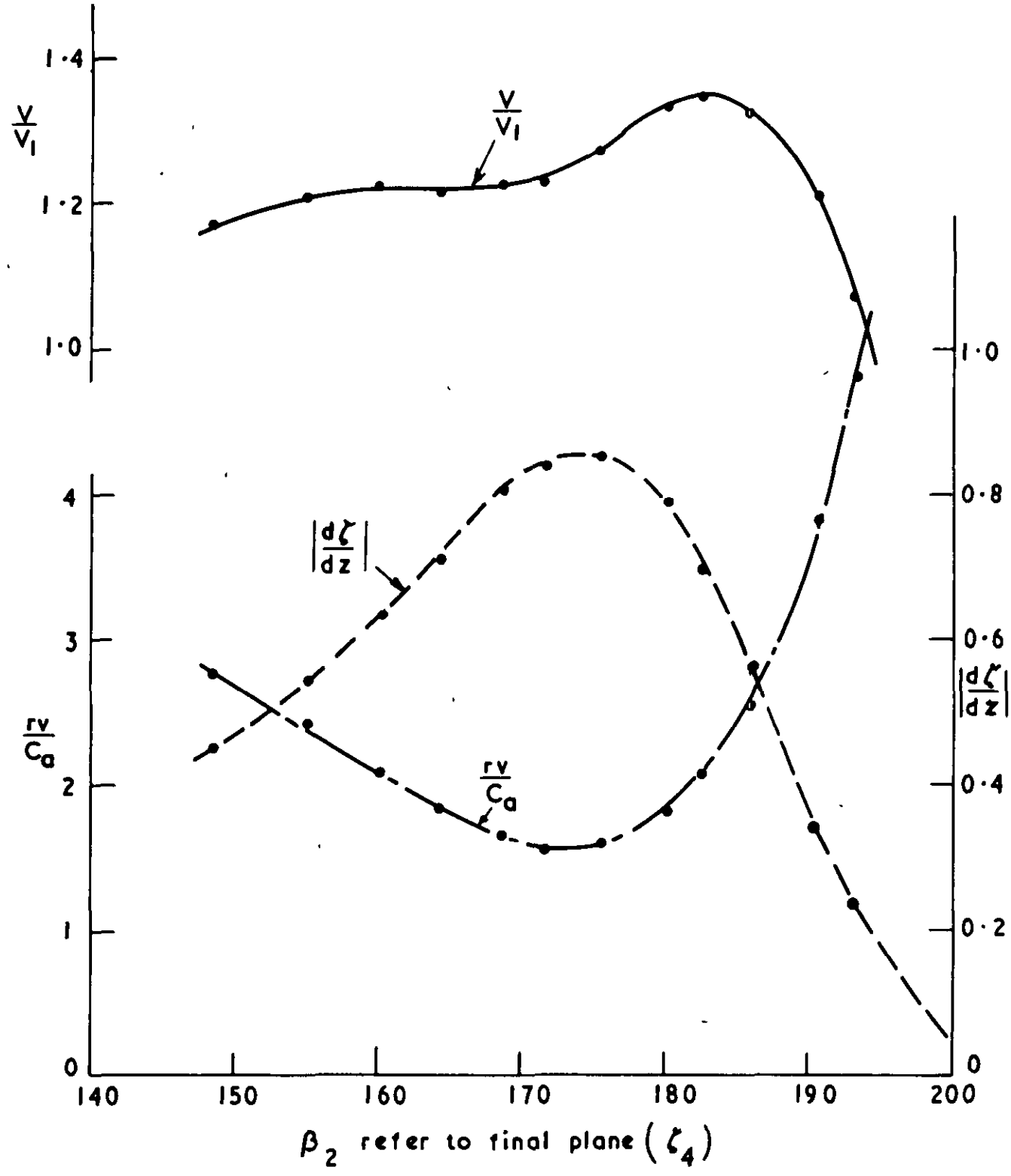

FIG. 23 Typical velocity curve near L.E. (Prog. 6/31/40)

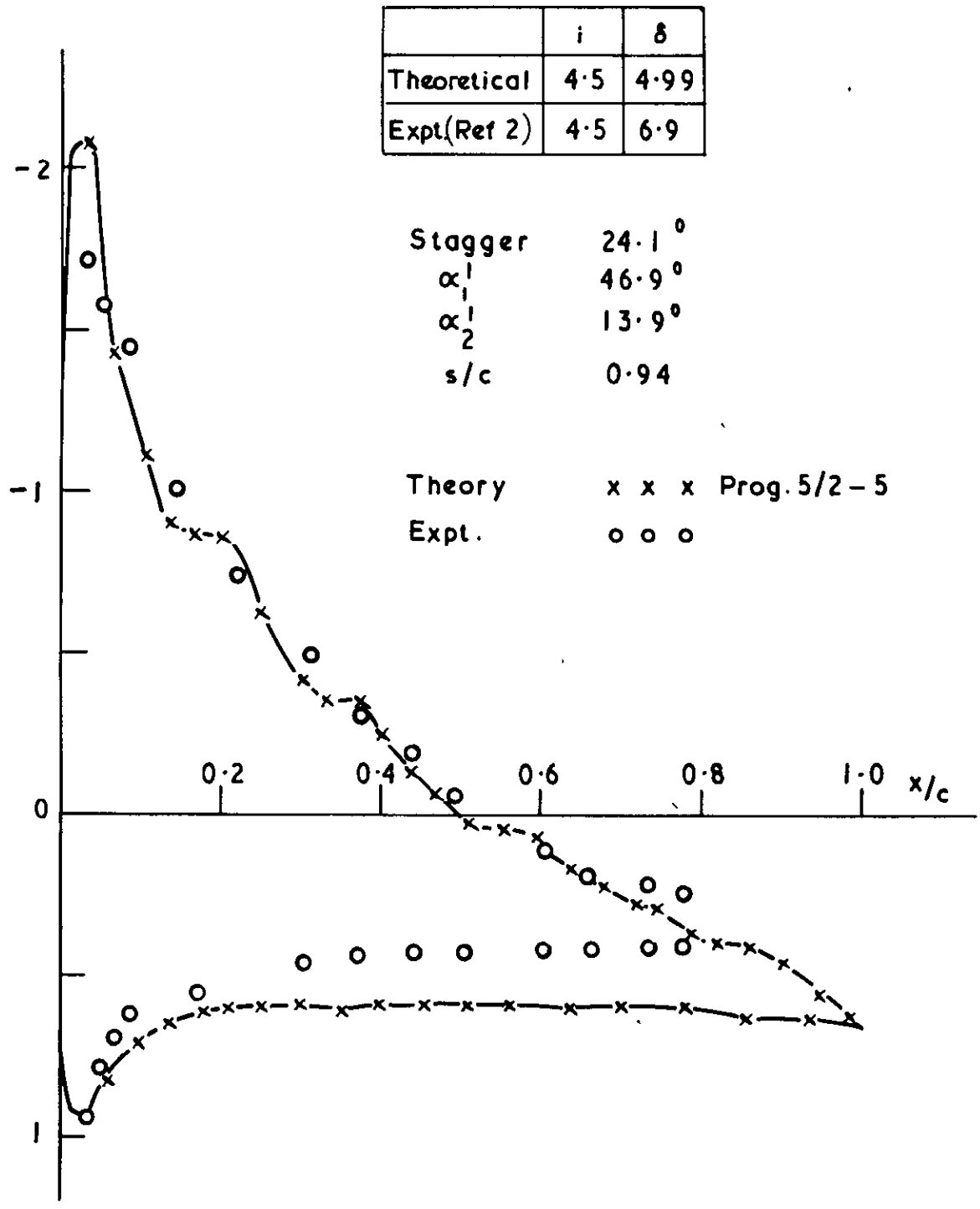

FIG. 24 Pressure distribution

II C2/.33 P40

A.R.C. C.P. No. 971
December, 1965
Yip, Y. M. and Railly, J. W.

POTENTIAL FLOW THEORY FOR TANDEM CASCADE BY HOWELL'S METHOD

The solution of a tandem cascade is obtained by replacing the second blade by singularities (two in this case), and carrying out an exact conformal transformation of the first blade by Howell's method. A digital computer programme which deals with the numerical work of the final Kármán-Theodorsen transformation in a new way is described.

A.R.C. C.P. No. 971
December, 1965
Yip, Y. M. and Railly, J. W.

POTENTIAL FLOW THEORY FOR TANDEM CASCADE BY HOWELL'S METHOD

The solution of a tandem cascade is obtained by replacing the second blade by singularities (two in this case), and carrying out an exact conformal transformation of the first blade by Howell's method. A digital computer programme which deals with the numerical work of the final Kármán-Theodorsen transformation in a new way is described.

A.R.C. C.P. No. 971
December, 1965
Yip, Y. M. and Railly, J. W.

POTENTIAL FLOW THEORY FOR TANDEM CASCADE BY HOWELL'S METHOD

The solution of a tandem cascade is obtained by replacing the second blade by singularities (two in this case), and carrying out an exact conformal transformation of the first blade by Howell's method. A digital computer programme which deals with the numerical work of the final Kármán-Theodorsen transformation in a new way is described.

DETACHABLE ABSTRACT CARDS

Published by
HER MAJESTY'S STATIONERY OFFICE

To be purchased from
49 High Holborn, London W C.1
423 Oxford Street, London W 1
13A Castle Street, Edinburgh 2
109 St Mary Street, Cardiff
Brazennose Street, Manchester 2
50 Fairfax Street, Bristol 1
35 Smallbrook, Ringway, Birmingham 5
7-11 Linenhall Street, Belfast 2
or through any bookseller

C.P. No. 971

S.O. CODE No. 23-9017-71